

Durham E-Theses

Investigating the Potential of Bacteriophage Proteins Kil and NinH as Novel Antibacterials

KUSZYNSKI, ELEANOR,PHILIPPA,FIONA

How to cite:

KUSZYNSKI, ELEANOR,PHILIPPA,FIONA (2025) *Investigating the Potential of Bacteriophage Proteins Kil and NinH as Novel Antibacterials*, Durham theses, Durham University. Available at Durham E-Theses Online: <http://etheses.dur.ac.uk/16058/>

Use policy

The full-text may be used and/or reproduced, and given to third parties in any format or medium, without prior permission or charge, for personal research or study, educational, or not-for-profit purposes provided that:

- a full bibliographic reference is made to the original source
- a [link](#) is made to the metadata record in Durham E-Theses
- the full-text is not changed in any way

The full-text must not be sold in any format or medium without the formal permission of the copyright holders.

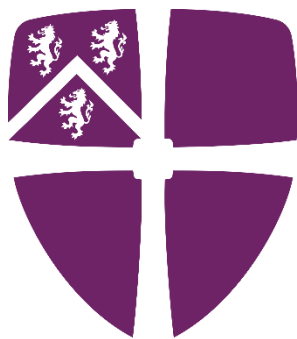
Please consult the [full Durham E-Theses policy](#) for further details.

Investigating the Potential of Bacteriophage Proteins Kil and NinH as Novel Antibacterials

Eleanor Philippa Fiona Kuszynski

Supervisors: Dr Gary Sharples, Dr Liz Morris

Thesis submitted for the degree of Master of
Science, by Research



Durham
University

Department of Biology

Durham University

2024

Abstract

Antibiotic resistance is a significant global health concern caused by the misuse and overuse of the existing repertoire of drugs. To combat this growing problem, alternative approaches to treat the rise of antibiotic resistant pathogenic bacteria are required. Bacteriophages, used for phage therapy to treat infections themselves, and the proteins they encode are a potential source of novel antibacterials. Embedded within these phage genomes are short polypeptides, called Kil proteins, that all appear to impact bacterial viability by blocking cell division. FtsZ, involved in Z-ring formation and essential for bacterial cell division, is known to be a target for at least some of these Kil proteins. Another gene product of interest, from bacteriophage λ , is NinH, which has DNA binding and bending properties and can also induce detrimental cell filamentation. It shares sequence and functional similarities with Fis, a bacterial nucleoid-associated protein, which plays a role in chromosome condensation, transcriptional regulation and phage site specific integration/excision reactions. In this thesis, I have studied the toxicity of Kil proteins expressed in *Escherichia coli*, examined their predicted structures and potential for interactions with FtsZ. I have also attempted to further understand the function of NinH and its negative effects on *E. coli* cell morphology. Both the Kil and NinH proteins have potential in helping to combat antibacterial resistance through novel mechanisms of cell toxicity.

Contents

Investigating the Potential of Bacteriophage Proteins Kil and NinH as Novel Antibacterials	1
Abstract	2
List of Figures	6
List of Tables	10
Abbreviations	11
Declaration	13
Statement of Copyright	13
Acknowledgements	14
1. Introduction	15
1.1 <i>Escherichia coli</i> bacterial cell division	17
1.2 FtsZ structure and function.....	18
1.3 FtsZ regulatory systems.....	19
1.4 Existing FtsZ-targeting drugs	21
1.5 Bacteriophages	21
1.6 Kil proteins	23
1.7 Fis	24
1.8 NinH	26
1.9 Thesis overview.....	28
2. Materials & Methods.....	30
2.1 Bacterial strains & growth conditions	30

2.2 Bacterial viability assays	32
2.3 Protein overexpression	32
2.4 SDS-PAGE	33
2.5 Protein purification.....	34
2.6 Protein dialysis	35
2.7 Size exclusion chromatography.....	35
2.8 Bioinformatics analysis	36
2.9 Microscopy	36
3. Results	38
3.1 Antibacterial activity of Kil proteins	38
3.2 Protein overexpression	41
3.3 Protein purification.....	43
3.4 Protein:protein interaction assay	47
3.5 AlphaFold models.....	48
3.6 Kil proteins analysed on the Dali server	54
3.7 Examination of the in vivo role of phage λ NinH	56
4. Discussion	61
4.1 λ Kil.....	61
4.2 Mu Kil	63
4.3 Rac Kil.....	64
4.4 P22 Kil.....	66

4.5 DicB.....	67
4.6 YdfD	68
4.7 T7 Gp0.4.....	70
4.8 NinH and <i>E. coli</i> cell elongation	72
5. Conclusions & future work	74
6. References	76

List of Figures

Figure 1: Stages of <i>E. coli</i> divisome construction. Proto-ring assembly is accompanied by the recruitment of the FtsE-FtsX complex and FtsK which coordinates chromosome segregation with cell division. The FtsQ-FtsL-FtsB complex is then recruited which in turn is important for recruitment and activation of FtsI (septum specific transpeptidase) and FtsW (glycosyltransferase). FtsN then binds and activates FtsI-FtsW enzymatic activity. Taken from Cameron and Margolin, 2024.	18
Figure 2: Formation and role of the Z-ring and regulatory systems during binary fission of <i>E. coli</i> . Created using BioRender.com.	20
Figure 3: Model of phage lifecycle, entering either the lytic or lysogenic cycles. Adapted from Brady et al., 2021. Created with BioRender.com.	22
Figure 4: Consensus binding site of <i>E. coli</i> Fis. Base pairs necessary for Fis recognition are highlighted. Taken from Chakraborti et al., 2020.	25
Figure 5: Similarity between of <i>E. coli</i> Fis and phage λ NinH. a) Structure of the Fis homodimer bound to its consensus DNA (Chakraborti et al., 2020). b) Structure of a monomer of NinH as predicted by AlphaFold showing the three helices (AlphaFold2.ipynb - Colaboratory (google.com)).	26
Figure 6: The NinH recognition sequence determined by a high-throughput-systematic evolution of ligands by an exponential enrichment method (Chakraborti et al., 2020).	28
Figure 7: Bacterial viability assays of transformed BL21-AI. Strains labelled along the top, y-axis shows the culture dilutions. Top, uninduced agar plates + antibiotic. Bottom, induced agar plates + antibiotic + 1mM IPTG + 0.2% L-Arabinose.....	39
Figure 8: <i>E. coli</i> viability following expression of phage polypeptides. y-axis colony forming units (CFU) per millilitre, x-axis strain labels. Bacteria carrying constructs	

expressing phage genes were cultivated in LB media and diluted cultures applied to LB agar plates with and without addition of IPTG and arabinose. Results are the mean and standard deviation of independent experiments performed in triplicate.40

Figure 9: 8-16% gradient polyacrylamide gels showing small-scale overexpression of uninduced (-) and induced (+) Kil proteins. Gels were stained in Coomassie Brilliant Blue.42

Figure 10: 8-16% SDS-PAGE of Kil proteins isolated by nickel-affinity chromatography stained by Coomassie Brilliant Blue. Uninduced (-) and induced (+) E. coli BL21-AI carrying plasmids expressing Kil proteins were lysed and pellet (P) and supernatant (S) separated. The flow through (FT) from the nickel-sepharose column was collected and fractions (1-6) collected following elution. Red arrows indicate expected molecular weight.44

Figure 11: 8-16% SDS-PAGE of Kil proteins purified by nickel-affinity chromatography after denaturation with urea. Stained by Coomassie Brilliant Blue. Uninduced (-) and induced (+) E. coli BL21-AI carrying plasmids expressing Kil proteins were lysed and pellet (P) and supernatant (S) separated. The flow through (FT) from the nickel-sepharose column was collected and fractions (1-6) collected following elution. Red arrows indicate expected molecular weight.45

Figure 12: 8-16% SDS-PAGE of purified and dialysed Kil proteins stained with Coomassie Brilliant Blue. Uninduced (-) and induced (+) E. coli BL21-AI carrying plasmids expressing Kil proteins.46

Figure 13: Size exclusion chromatography graphs. a) FtsZ b) Rac Kil c) FtsZ+Rac. FtsZ has a broad peak over multiple elutions. Rac Kil has a sharper peak indicative of a small protein of the expected molecular weight. FtsZ + Rac Kil has a broad peak

again but with several discrete peaks however it cannot be distinguished if there has been an interaction between FtsZ and Rac Kil.....48

Figure 14: 3D-structural models of Kil proteins produced using AlphaFold2 Colab. Colour on the models corresponds to pLDDT score, indicating confidence in the structure. a) λ Kil, b) Mu Kil, c) Rac Kil, d) DicB, e) YdfD, f) P22 Kil, g) T7 Gp0.450

Figure 15: AlphaFold models of FtsZ and Kil protein interactions. Colour on the models corresponds to pLDDT score, indicating confidence in the structure. a) Lambda Kil, b) Mu Kil, c) Rac Kil, d) DicB, e) YdfD, f) P22 Kil and g) Gp0.4.52

Figure 16: AlphaFold models showing FtsZ (cyan) and Kil protein (green) potential interactions with FtsZ residues L169 and V208 shown in red. Imaged from PyMOL. a) λ Kil, b) Mu Kil, c) Rac Kil, d) T7 Gp0.4.....53

Figure 17: Predicted aligned error (pAE) for the corresponding AlphaFold models. The lower the predicted aligned error the darker shade of blue.....54

Figure 18: Pairwise structural alignment of Rac Kil and eif5A. Upper block showing amino acid sequence, lower block secondary structure states L = Coil, H = Helix and E = Sheet.55

Figure 19: DALI server 3D-superimposition of Rac Kil (green) and eif5A (orange). Structural models from AlphaFold (Rac Kil) and the PDB (eif5A) were used.55

Figure 20: Correspondence analysis taken from DALI server. x and y axes showing similarity through structural neighbourhoods.56

Figure 21: a) Images of uninduced and induced E. coli cells for each strain. b) Box and whisker plots. Blue = uninduced, Orange = induced. Y-axis showing cell length57

Figure 22: DNA stained with DAPI showing distribution during division a) Uninduced LT2230 b) uninduced LT2260 c) uninduced LT2259. Grey values were measured along the long axis of the cells. Scale bar 10 μm59

Figure 23: DNA stained with DAPI showing distribution of DNA during division. a) uninduced LT447 b) induced LT447. Grey values were measured along the long axis of the cells. Scale bar 10 μm60

Figure 24: FtsZ (cyan) and Gp0.4 (green) protein-protein interaction model. FtsZ residues N24, L178 and F182 (red).....71

List of Tables

Table 1: Recombinant plasmids for Kil expression used in this study. Vector sequences that encode an N-terminal histidine-tag are highlighted in red.....	30
Table 2: <i>E. coli</i> strains used in testing of NinH	31
Table 3: Kil Protein concentrations after dialysis	47

Abbreviations

Antimicrobial resistance (AMR)

Antibacterial resistance (ABR)

Bicyclomycin (BCM)

Colony Forming Units (CFU)

C-terminal tail (CTT)

C-terminal variable region (CTV)

Eukaryotic Translation Initiation Factor 5A (eif5A)

Filamentous temperature sensitive mutant Z (FtsZ)

Flow Through (FT)

Förster Resonance Energy Transfer (FRET)

Helix-Turn-Helix (HTH)

High-throughput screening (HTS)

His-Wash Buffer (HWB)

His-Elute Buffer (HEB)

Isopropyl β -D-Thiogalactoside (IPTG)

L-arabinose (Ara)

Laser Scanning Confocal Microscopy (LSCM)

Luria-Bertani (LB)

Methylerythritol 2,4-cyclodiphosphate (HMBPP)

Minicell (Min)

Natural Product (NP)

Nucleoid Associated Proteins (NAPs)

Nucleotide occlusion (NO)

Protein Data Bank (PDB)

Predicted aligned error (pAE)

Predicted local difference test (plDDT)

Sodium dodecyl-sulphate polyacrylamide gel electrophoresis (SDS-PAGE)

Tandem-affinity purification (TAP)

2-C-methyl-D-erythritol 4-phosphate (MEP)

Declaration

I declare that, to the best of my knowledge, all work contained in this thesis is my own except where due reference or acknowledgement is given in the text and that this thesis has not been previously submitted to any other university for a higher qualification.

Statement of Copyright

The copyright of this thesis rests with the author. No quotation from it should be published without the author's prior written consent and information derived from it should be acknowledged.

Acknowledgements

I'd like to give a huge thank you to my supervisor Dr Gary Sharples and all the members of the Sharples group for their support over the past two years. And a massive thank you to Adam, Barney, Chris, Lizzie, Lucy and Mum for their patience in listening to me go on about my project!

1. Introduction

Antimicrobial resistance (AMR) is increasingly becoming a serious global health challenge. A United Kingdom government-commissioned report (O'Neill, 2016) stated that without urgent action by 2050, 10 million people will die annually as a consequence of AMR. In the United States, 20% of hospitalisations annually are due to infections caused by multidrug resistant bacteria (Fong, 2023). While AMR is a natural process, the overuse of antimicrobials by humans is increasing the selection pressure and rate at which AMR occurs (Michael, Dominey-Howes and Labbate, 2014). Antibiotic over-prescription in clinical settings alongside prophylactic and routine-drug treatment of livestock are two of the leading factors responsible for this rise. Drug resistant microbes make treatment of the infections they cause increasingly difficult with our existing selection of antibiotics. The current rate of development of new antibiotics in the traditional mould is unlikely to outpace the rise in resistance (Christopher et al., 2021). Alternative approaches and novel compounds are urgently needed to combat this problem.

Throughout human history microbes with antibacterial properties have been harnessed in the treatment of infections. Some of the earliest known examples were poultices composed of mouldy bread used to treat open wounds as documented in the Ebers papyrus, dating back to 1550 BC (Haas, 1999). Over the last century there was an explosion in the discovery of antibacterial compounds. Salvarsan (an arsenic-based pro-drug) was the first synthetic chemotherapeutic agent and was employed in the treatment of *Treponema pallidum*, the causative agent of syphilis (Gelpi, Gilbertson and Tucker, 2015). Salvarsan was replaced by sulphonamides which proved to be effective against a broader spectrum of microbials and with considerably reduced toxicity (Hutchings, Truman and Wilkinson, 2019). This was followed by the

discovery of penicillin, a natural product (NP) produced by fungi from the *Penicillium* genus (Fleming, 1929). Significantly, the determination of its chemical structure led to the development of numerous β -lactam derivatives which proved highly effective against resistant strains (Hutchings, Truman and Wilkinson, 2019).

The “golden age” of antibiotic discovery lasted from the 1940s through to the 1960s (Hutchings, Truman and Wilkinson, 2019). During this period many new NP antibiotics were identified, many still in use today; however, their efficacy is hampered by antibiotic resistance – in part due to their excessive use (Katz and Baltz, 2016). Since then, the antibiotic discovery pipeline has faltered and there have been few novel antibiotic drugs that have successfully reached the clinic. Often those that do make it past the clinical trials are derivatives of known NPs or synthetic compounds (Katz and Baltz, 2016). Despite recent investment in high-throughput screening (HTS) programmes, antimicrobial drug discovery remains challenging. AstraZeneca conducted 65 HTS campaigns which had some successes, however, no compounds were identified with activity against multidrug-resistant Gram-negative bacteria (Tommasi et al., 2015). Similarly, over a seven-year period, GlaxoSmithKline conducted 70 HTS campaigns involving over 500,000 compound candidates, but none were put forward for development (Payne et al., 2015). These failures further stress the need for novel antibiotics from alternative sources.

As stated by the O’Neill report, a key step in overcoming antibacterial resistance (ABR) is increased research into novel antibacterial agents, while continuing to improve and protect the usage of existing ones. Current drugs frequently target key bacterial processes, typically cell wall assembly, folate biosynthesis, nucleic acids or specific essential proteins (Lock and Harry, 2008). The issue with modifying existing antibiotics is that the mechanism of killing remains the same, so resistance to these

drugs tends to occur more rapidly. To circumvent this problem, focus is shifting onto alternative cellular targets essential for bacterial survival. One such target is Filamentous temperature-sensitive mutant Z (FtsZ), a highly-conserved essential cell division protein found in almost all bacterial species.

1.1 *Escherichia coli* bacterial cell division

Despite decades of research, a complete picture of bacterial cell division remains elusive. However, *Escherichia coli*, as a representative Gram-negative, is one of the best characterised bacterial species in this regard. *E. coli* is a rod-shaped bacterium, and undergoes binary fission at the mid-point of the growing parent cell and ultimately divides into two daughter cells. Failure to divide results in cell filamentation and eventual death. Cell division in *E. coli* is implemented by the divisome, a multi-protein trans-envelope complex. FtsZ is a cytoplasmic tubulin-like GTP-hydrolase and the first protein to localise at the site of division – the mid-cell (Romberg and Levin, 2003). FtsZ monomers undergo head-to-tail polymerisation forming protofilaments. These filaments laterally bond to others forming a discontinuous ring-like structure, the Z-ring (Erickson, Anderson and Osawa, 2010). The Z-ring is then anchored to the cytoplasmic membrane via ZipA – a transmembrane protein – and additional supplementary membrane associated proteins, including FtsA (Figure 1). This anchored structure is known as the proto-ring (Huang, Durand-Heredia and Janakiraman, 2013) which directs recruitment and assembly of FtsK, FtsQ, FtsL, FtsB, FtsW, FtsI and FtsN. These accessory proteins are critical for the structural remodelling and regulation of the cell wall during division (Figure 1).

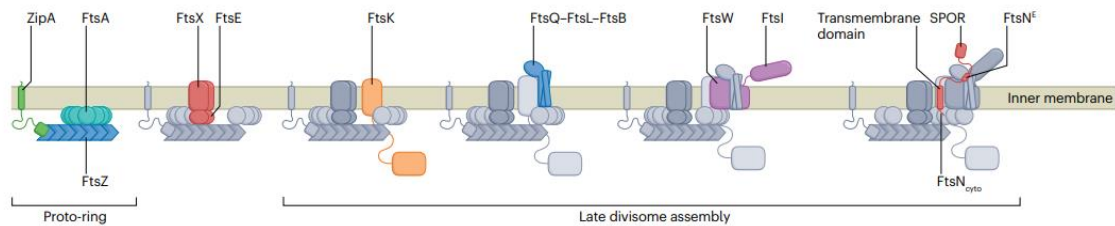


Figure 1: Stages of *E. coli* divisome construction. Proto-ring assembly is accompanied by the recruitment of the FtsE-FtsX complex and FtsK which coordinates chromosome segregation with cell division. The FtsQ-FtsL-FtsB complex is then recruited which in turn is important for recruitment and activation of FtsI (septum specific transpeptidase) and FtsW (glycosyltransferase). FtsN then binds and activates FtsI-FtsW enzymatic activity. Taken from Cameron and Margolin, 2024.

Once the core essential proteins achieve critical threshold concentrations within the divisome, a conformational change triggers activation of peptidoglycan cell wall synthesis (Egan and Vollmer, 2013). Treadmilling of FtsZ polymers aids the uniform distribution of peptidoglycan synthesis enzymes around the septum (Bisson-Filho et al., 2017). Cross wall synthesis drives constriction and other proteins complete the ordered infolding of the outer membrane. Division is completed with divisome disassembly and daughter cell separation (Natale, Pazos and Vicente, 2013).

1.2 FtsZ structure and function

FtsZ is a cell division protein that is highly conserved (40-50% sequence identity) among bacterial species, with only a few exceptions (Vaughan et al., 2004). Although its homology to eukaryotic counterparts is low, only 20% sequence identity at the protein level, it is a recognised functional homologue of the cytoskeletal protein tubulin. The ubiquity of FtsZ across most bacteria along with its absence in eukaryotes, makes it an attractive target for antibacterial drugs with reduced cytotoxicity in humans (Han et al., 2021).

FtsZ possesses five discrete domains: a poorly conserved N-terminal domain, a globular highly-conserved core, an unstructured C-terminal linker, a short C-terminal tail (CTT) and a C-terminal variable region (CTV) (Buske and Levin, 2012). The

globular core contains a GTP binding site and a T7 loop required for GTP hydrolysis. The CTT is involved in modulation of FtsZ, being able to associate with the membrane-associated proteins ZipA and FtsA (Figure 1). Monomers of FtsZ rely on GTP-dependent head-to-tail polymerisation to form protofilaments with one subunit's T7 loop inserted into the GTP-binding domain from another subunit, creating a GTPase active site (Schumacher et al., 2020).

1.3 FtsZ regulatory systems

The positioning of the Z-ring is tightly regulated, with only a 2% deviation off the mid-cell found in its placement in *E. coli* (Migocki et al., 2002). The regulatory systems, nucleotide occlusion (NO) and minicell (Min), direct this positioning (Rowlett and Margolin, 2015). In the Gram-positive *Bacillus subtilis*, the NO system utilises Noc to prevent premature division when nucleoids are unsegregated (Wu et al., 2009). There are 74 binding sites on the chromosome where Noc can assemble and it is thought that the physical presence of Noc prevents assembly of the divisome (Wu et al., 2009). However, in *E. coli*, the NO system utilises SlmA which also binds at sites on the chromosome, but has also been reported to associate with the FtsZ CTT thus disrupting Z-ring formation (Silber et al., 2020). The Min system prevents FtsZ assembly near the cell poles (Lutkenhaus, 2007). In *E. coli* the Min system comprises MinC, MinD and MinE (De Boer, Crossley and Rothfield, 1989). MinC directly interacts with FtsZ, preventing lateral interactions with other protofilaments and causing them to be shorter and curved (Dajkovic et al., 2008). MinC associates with MinD to form a membrane bound complex, which is spatially controlled by MinE (de Boer, Crossley and Rothfield, 1989). MinE migrates from pole to pole along with MinD, forming a zone of high MinC density at each pole. This ensures that FtsZ filament formation is restricted to the mid-cell region (Figure 2; Fu et al., 2001).

Interestingly, even when both of these systems are eliminated in *B. subtilis*, Z-rings can still form at the mid-cell (Rodrigues and Harry, 2012). Hence, other uncharacterised regulatory systems remain to be discovered, potentially akin to those found in other bacterial species which lack NO and Min (Migocki et al., 2002). FtsZ assembly can also be blocked by Sula during the SOS response (Bi and Lutkenhaus, 1993). The SOS response is activated if bacteria detect damage to their DNA. This response induces expression of Sula in order to inhibit cell division and gives the bacteria time to repair any chromosomal DNA damage that could interfere with normal genome segregation. Sula reversibly sequesters FtsZ monomers, disrupting

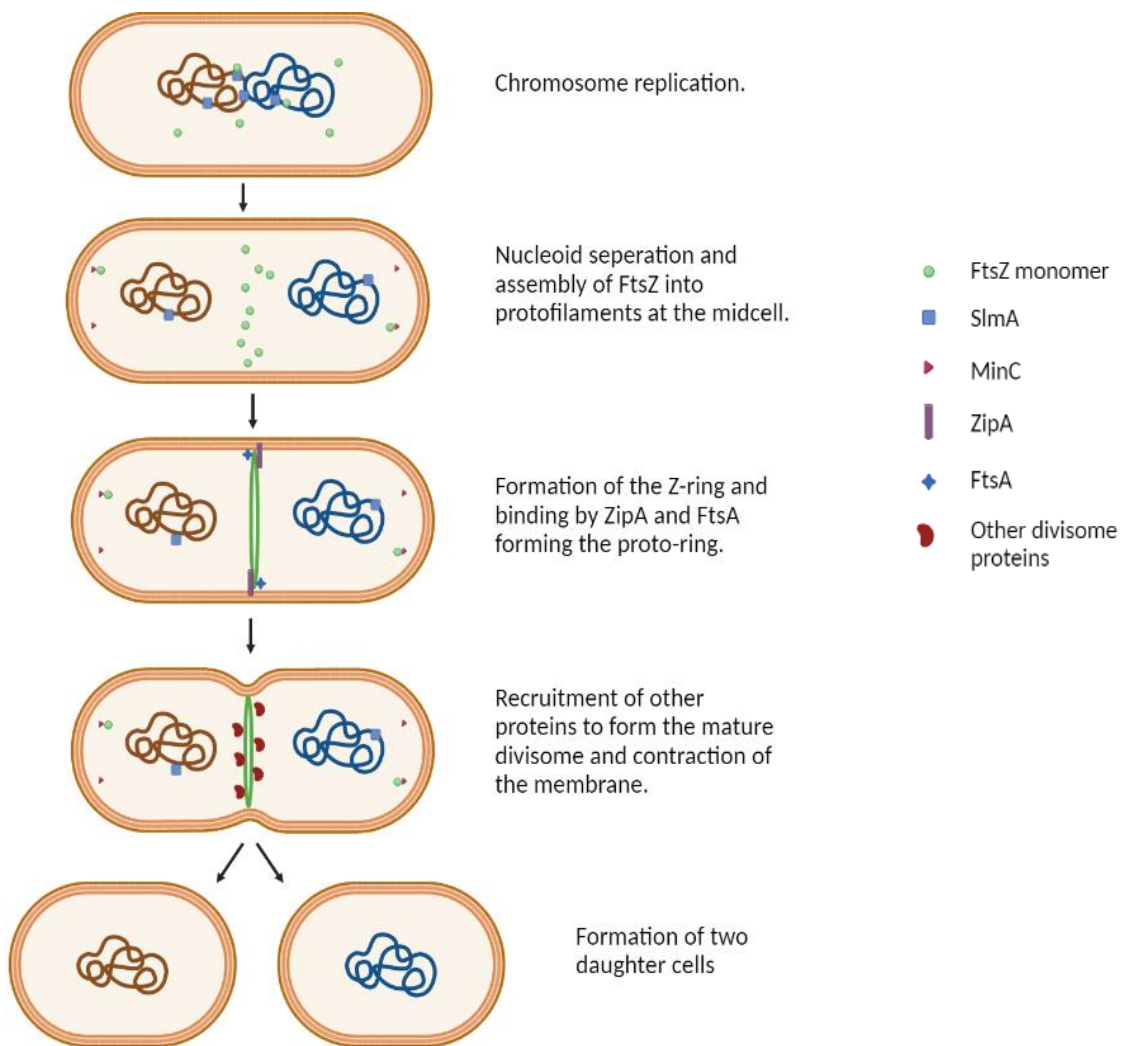


Figure 2: Formation and role of the Z-ring and regulatory systems during binary fission of *E. coli*. Created using BioRender.com.

polymerisation and reducing GTPase activity (Chen, Milam and Erickson, 2012). Irregular inhibition of FtsZ leads to continual cell elongation, bacterial filamentation and eventually cell death (Chen, Milam and Erickson, 2012). Given the essential role fulfilled by FtsZ in bacterial cell division, it has significant potential as a new target for a new class of antibacterial agents.

1.4 Existing FtsZ-targeting drugs

While several FtsZ inhibitors have been trialled for their efficacy against several bacterial species, only one compound has completed phase 1 clinical trials – TXA709 (Kusuma et al., 2019). TXA709 is a small, benzamide molecule that only appears to inhibit Gram-positive bacteria (Kaul et al., 2015). These drugs were designed to target the interdomain cleft of FtsZ, thus disrupting GTP binding (Fujita et al., 2017). The emergence of resistance has been problematic for such compounds (Kusuma et al., 2019), although promising synergistic effects were noted when TXA707 (the active product of TXA709) was combined with cefdinir (Kaul et al., 2016). This reduced the likelihood of resistance mutations arising to undetectable levels (Kaul et al., 2016) and suggests that a combinatorial approach that targets different components of the divisome may prove successful.

1.5 Bacteriophages

Bacteriophages (or phages) are ubiquitous killers of bacteria and outnumber them 10-fold, with an estimated 10^{30} phages predicted to occur across the globe (Chibani-Chennoufi et al., 2004). Prior to the discovery of penicillin and the widespread deployment of antibiotics, phage therapy was used as a treatment for a variety of infectious diseases, such as *Shigella dysenteriae* (Brüssow, 2005).

Depending on life cycle, phages can be classified as either virulent or temperate (Figure 3). A phage first recognises and binds to receptors on the bacterial cell surface and conformational changes upon contact trigger injection of their genetic material (Molineux and Panja, 2013). Virulent phages promptly enter the lytic cycle where they hijack the bacterial cell machinery to produce more phage particles (McNair, Bailey, and Edwards, 2012). Cell lysis is achieved by holin-endolysin systems (Catalao et al.,

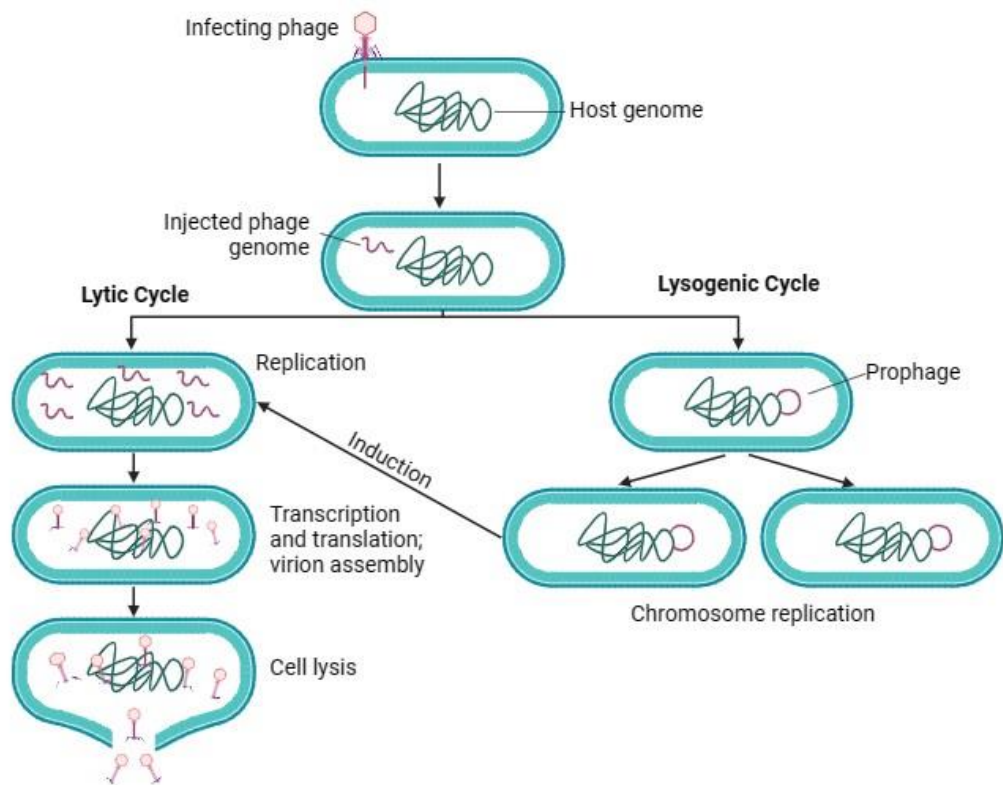


Figure 3: Model of phage lifecycle, entering either the lytic or lysogenic cycles. Adapted from Brady et al., 2021. Created with BioRender.com.

2013), leading to phage release and dissemination. Temperate phages can enter the lytic or lysogenic cycle and will do so depending on the surrounding environmental conditions (McNair, Bailey, and Edwards, 2012). In the lysogenic cycle, phages insert their genome into the host's chromosomes (Echols, 1972) and the integrated phage is known as a prophage. Prophages can re-enter the lytic cycle following excision from the host genome (Brady et al., 2021).

Cryptic prophages (defective prophages), consist of segments of phage DNA that have been integrated into bacterial chromosomes but have lost the capacity to excise. It is estimated that prophage genes constitute around 10-20% of bacterial genetic content (Lu et al., 2022). The *E. coli* K-12 genome was the first found to contain phage genes (Lederberg and Lederberg, 1953) and carries at least 10 defective prophages (Blattner et al., 1997). Expression of defective prophage genes is frequently repressed because of remnant functional repressors or the loss of suitable promoters, however, some can perform useful functions, while others may be toxic if expressed (Rueggeberg et al., 2015).

Defective phages and the products they encode could be a source of new antibacterials to combat ABR. By studying the mechanism of killing from these new potential sources we might uncover not just novel treatments but also discover new targets for drug development.

1.6 Kil proteins

Bacteriophage λ has been well documented to induce bacterial cell death and lysis in *E. coli* (Casjens and Hendrix, 2015). Through a defective prophage it was also discovered that phage λ can trigger cell filamentation and death by autolysis (Sergueev et al., 2001). This defective prophage contained only the P_L operon and the immunity region. By deletion of successive genes within the prophage, the gene responsible for cell death was identified and termed *kil* (host killing by an induced lambda prophage) (Greer, 1975). The *kil* gene was presumed to encode a protein which targeted a component of the bacterial cell division apparatus due to the substantial levels of cell filamentation and the loss of viability after induction (Sergueev et al., 2002). The mechanism was eventually investigated further and λ Kil found to block FtsZ-ring

formation in *E. coli* (Haeusser et al., 2014). It did not appear to act by altering levels of FtsZ or manipulation of the endogenous regulatory systems, such as NO, Min and Sula (Haeusser et al., 2014). However, mutants resistant to λ Kil were also resistant to inhibition by Min and Sula (Haeusser et al., 2014). Additional experiments eventually determined that resistance to Kil was due to a lack of ZipA and taking this further λ Kil was found to interact with both ZipA and FtsZ (Haeusser et al., 2014). Further studies revealed that λ Kil preferentially binds to FtsZ-GDP monomers and thereby acts through a similar sequestration mechanism to Sula (Hernández-Rocamora et al., 2015).

Several lytic peptides with similar effects to λ Kil have been identified in other phages and prophages, notably Mu, P22, Qin, Rac and T7. P22 Kil, Rac Kil and T7 Gp0.4 apparently function in a similar way to λ Kil (Haeusser et al., 2014; Semerjian, Malloy and Poteete, 1989; Kiro et al., 2013). Mu Kil instead of leading to cell elongation, triggers cell rounding but still induces lysis (Waggoner et al., 1989). From *E. coli* prophage Qin, DicB and YdfD are potential inhibitors of the divisome (Faubladier and Bouché, 1994). DicB affects the Min system, thus blocking septum formation, whereas the product of *ydfD*, located immediately downstream of *dicB*, uses an uncharacterised mechanism which requires normal cell division to occur in order to induce lysis (Masuda, Awano and Inouye, 2016). Recent work suggests that YdfD acts upon IspG, a key enzyme within the 2-C-methyl-D-erythritol 4-phosphate (MEP) pathway (Lu et al., 2022). Currently there is a single drug, fosmidomycin, under clinical investigation as an inhibitor of the MEP pathway (Borrmann et al., 2006).

1.7 Fis

Supercoiling, RNA and nucleoid associated proteins (NAPs) are all responsible for compaction of the bacterial chromosome into a nucleoid (Amemiya, Schroeder and

Freddolino, 2021). Different NAPs play crucial roles in gene regulation alongside their functions in chromosome condensation (Browning, Grainger and Busby, 2010).

Fis is one such NAP that contributes to: chromosome condensation, transcriptional regulation and phage site specific integration/excision reactions and is most abundantly expressed under rapid growth conditions (Cho et al., 2008). Fis bends DNA by non-specific binding to segments of 21 bp in length and then bending the



Figure 4: Consensus binding site of *E. coli* Fis. Base pairs necessary for Fis recognition are highlighted. Taken from Chakraborti et al., 2020.

DNA by $\sim 65^\circ$ (Skoko et al., 2006; Stella, Cascio and Johnson, 2010). Despite being able to associate with so many targets non-specifically, Fis preferentially binds a pseudo-palindromic sequence with G/C inverted repeats separated by an AT rich core (Figure 4).

This allows it to form stable complexes with regions of the bacterial chromosome and globally influence gene expression of 923 genes during exponential growth (Cho et al., 2008). Fis identifies its targets through AT rich sites that form narrow minor grooves which then allows the Fis homodimer to make specific contacts with the adjacent major groove through the G/C pair (Stella, Cascio and Johnson, 2010). The Fis homodimer then draws the DNA over its two helix-turn-helix (HTH) motifs inducing a $\sim 65^\circ$ bend in the DNA (Stella, Cascio and Johnson, 2010) (Figure 5a). Excision of phage λ requires Fis binding to a segment of DNA within the *attR*

recombination site, which enhances binding of the phage excisionase Xis (Papagiannis et al., 2007).

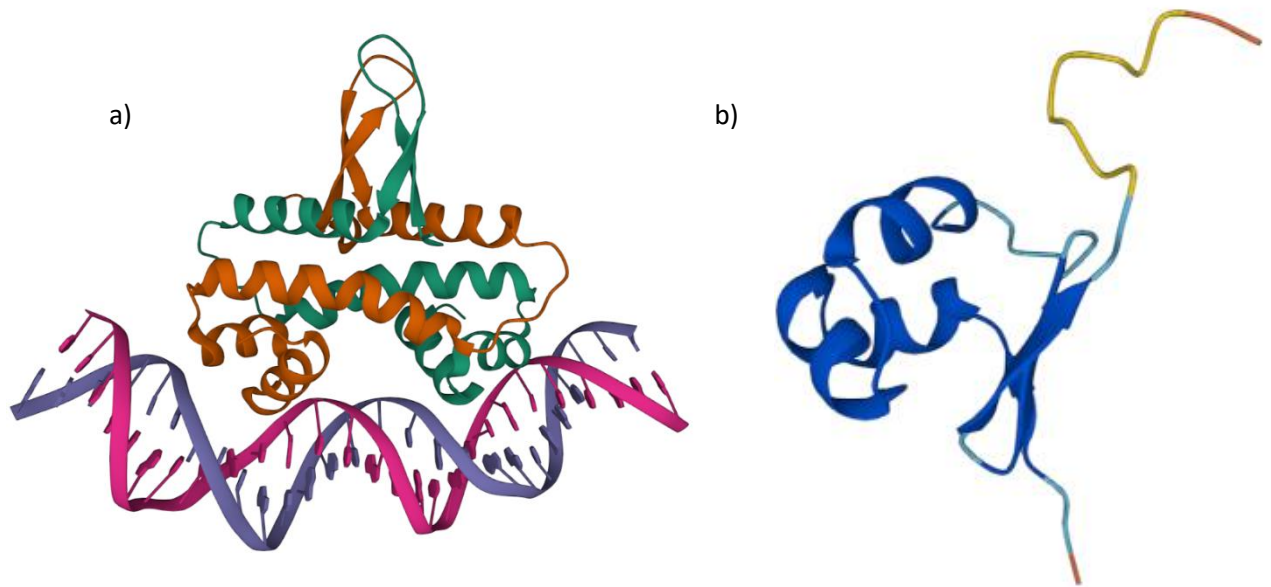


Figure 5: Similarity between of *E. coli* Fis and phage λ NinH. a) Structure of the Fis homodimer bound to its consensus DNA (Chakraborti et al., 2020). b) Structure of a monomer of NinH as predicted by AlphaFold showing the three helices ([AlphaFold2.ipynb - Colaboratory \(google.com\)](https://alphafold2.ipynb-colaboratory.google.com)).

1.8 NinH

Phage λ encodes a small protein, NinH, that shares sequence homology with Fis but, unlike Fis, is highly toxic when overexpressed (Chakraborti et al., 2020). Previous work using ribosome profiling found that NinH is exclusively expressed during the phage lytic cycle, as early as two minutes after prophage induction (Liu et al., 2013). NinH is 68-residues long and predicted to have a HTH motif from residues 17-38 (Figure 5b). *E. coli* Fis and λ NinH share 40% sequence identity and 67% similarity over this region. Out of eight residues in Fis that contact the DNA, seven are conserved in NinH (Chakraborti et al., 2020). The exception being Asn84 in Fis, which is represented by Ser29 in NinH. Asn84 is not necessary for high affinity DNA binding but does discriminate for binding when a thymine is present at -4/+4 in the 21 bp binding site (Stella, Cascio and Johnson, 2010). NinH residues 44-48 and 51-55 are

predicted to form β -sheets, potentially sharing a similarity with the N-terminal region of Fis. The NinH C-terminal tail is thought to contribute to dimerization, which has dimensions in small angle X-ray scattering of ~ 20 kDa similar to the structure of the Fis dimer (Chakraborti et al., 2020).

NinH preferentially binds dsDNA, forming two complexes on a 60 bp stretch of dsDNA (Chakraborti et al., 2020). NinH appears to show cooperative binding to dsDNA although there was no difference in affinity for branched DNA structures, including model replication forks and 4-stranded Holliday junctions. No change in binding affinity was detected with pre-kinked DNA, although formation of a second complex was consistent with cooperative assembly of a second NinH homodimer (Chakraborti et al., 2020).

The DNA bending capability of NinH was measured using Förster Resonance Energy Transfer (FRET). Upon addition of NinH to a linear 20 bp substrate, energy transfer efficiency increased – consistent with a shortening of the distance between the fluorophores at each end of the molecule. Bends of 35° to 46° were estimated to have formed. This is a shallower bend than Fis, which bends DNA between 50 - 90° , and 65° when co-crystallised with its cognate sequence (Pan et al., 1996; Stella, Cascio and Johnson, 2010). Chakraborti et al. (2020), suggested that the reduced bending capacity of NinH could be due to a different arrangement of the dimer with its substrate.

NinH preferentially associates with 15 bp sequences with similarity to Fis high-affinity binding sites. The preferred NinH sequence's signature (5'-G-N₁₃-C-3') matches that



Figure 6: The NinH recognition sequence determined by a high-throughput-systematic evolution of ligands by an exponential enrichment method (Chakraborti et al., 2020).

of Fis, although the central core sequence is less constrained to an AT-rich motif (Figure 6). The pseudo-palindromic motif fits with NinH homodimer assembly, allowing each HTH domain to interact with the major groove and indicates that both NinH and Fis bind in a similar fashion and could overlap in the sequences that they recognise *in vivo* (Chakraborti et al., 2020).

E. coli BL21-AI carrying pET-*ninH* constructs were used to evaluate toxicity. When appropriate inducers (arabinose and IPTG) used to activate gene expression were absent, all cells exhibited normal growth. In contrast, when *ninH* expression was induced from the constructs, bacterial cell growth was severely inhibited (Chakraborti et al., 2020). This decrease in growth was attributed to NinH interfering with normal chromosomal functionality through binding, since mutants defective in interactions with DNA had no detrimental effect on bacterial growth (Chakraborti et al., 2020).

1.9 Thesis overview

Novel antibacterials are desperately needed to treat increasingly antibiotic resistant bacteria. Several approaches are now being considered as an alternative to traditional antibiotics, including the use of phages or their products (Mdarhri et al., 2022). λ Kil, Mu Kil, Rac Kil, P22 Kil, Qin DicB, Qin YdfD and T7 Gp0.4 are all small polypeptides from the secondary phage lytic cycle that have already demonstrated

varying degrees of capability in killing *E. coli*. However, the precise mechanisms by which they work are still unknown. NinH has been recently found to be a protein which can bind and bend bacterial DNA and its overexpression is also toxic – however little is known about its role in cell death. Both the small peptides and NinH have potential as antibacterials, but before these proteins can be considered further, more information is needed on their modes of action.

This thesis aims to further characterise phage NinH and Kil proteins *in vivo* and *in vitro* to assess their potential as novel antibacterials and determine their specific functions. We hypothesise that NinH exhibits antibacterial activity due to its similarity to Fis in binding and bending bacterial DNA, thus causing aberrant chromosomal replication. We hypothesise that the Kil proteins' antibacterial activity is due to their ability to disrupt normal cell division by inhibiting Z-ring formation.

The main objectives were:

1. Determine the structure of Kil proteins and define their protein-protein interactions *in vitro* using size exclusion chromatography.
2. Identify cellular targets of NinH. This will be achieved through light microscopy to measure morphological changes between induced and uninduced constructs of NinH in *E. coli*.

2. Materials & Methods

2.1 Bacterial strains & growth conditions

All strains used for Kil experiments were obtained as pre-existing stocks of *E. coli* BL21-AI ($F^- ompT gal dcm lon hsdSB(r_B^- m_B^-) araB::T7RNAP-tetA$) transformed with pET plasmids containing recombinant phage genes to allow inducible *kil* expression (Table 1). The phage T7 Gp0.4 construct proved too toxic to be recovered in *E. coli*.

Table 1: Recombinant plasmids for Kil expression used in this study. Vector sequences that encode an N-terminal histidine-tag are highlighted in red.

Protein	Plasmid Vector	Antibiotic Resistance	Molecular Weight (kDa)	Protein Sequence
<i>E. coli</i> FtsZ	pET16b	Ampicillin	42.82	MGHHHHHHHHSSGHIEGRHMF ELTNDAVIKVIGVGGGGGNAVEHMVRERIEGVEFFAVNTDAQALRKTAVGQTIQIGSGITKGLGAGANPEVGRNAADEDRDALRAALEGADMVFIAAGMGGGTGTGAAPVVAEVAKDLGILTVAVVTKPFNFEGKKRMAFAEQGITELSKHVDSLITIPNDKLLKVLGRGISLLDAFGAANDVLKGAVQGIAELITRPLMNVDFAADVRTVMSEMGYAMMGSGVASGEDRAEEAAEMAISPLEDIDLSGARGVLVNITAGFDLRLDEFETVGNTRAFASDNATVVIGTSLDPDMNDELRVTVVATGIGMDKRPEITLVTKQVQQPVMDDRYQQHGMAPLTQEQQKPVAKVVNDNAPQTAKEPDYLDIPAFLRKQAD
Phage λ Kil	pET22b	Ampicillin	12.22	MGSSHHHHHHSSGLVPRGSHM PLQGGLLLAALPNLYLNESPVNYVTDGNALSTYLISQESQRMDQTLMAIQTKFTIATFIGDEKMFREAVDAYKKWILILKLRSKSIH
Phage Mu Kil	pET28a	Kanamycin	10.57	MGSSHHHHHHSSGLVPRGSHM ARNIKMATDAQNWLQARGSHVNESYLGVARPIL EITYPPVELVKN AVRIMEHKSGVARSVW TARLNGCQIIWR
Phage Rac Kil	pET28a	Kanamycin	10.59	MGSSHHHHHHSSGLVPRGSHM IAHFGTDEIPRQCVP GDYVLHEGRTYIASANNIKKRKLYIRNLTKTFITDRMIKVFLGRDGLPVKAESW
Phage P22 Kil	pET28a	Kanamycin	9.11	MGSSHHHHHHSSGLVPRGSHM TIVPVNGTILVQQGNREFNKLYEASFPDTKEGNSAAYAWASSIAMGWEDCQDEDWNRNHAA

Phage Qin DicB	pET28a	Kanamycin	9.12	MGSSHHHHHHSSGLVPRGSHMKLLP NVNTSEGCFEIGVTISNPVFTEDAIN KRKQERELLNKICIVSMLARLRLMPK GCAQ
Phage Qin YdfD	pET28a	Kanamycin	9.00	MGSSHHHHHHSSGLVPRGSHMNSAFV LVLTVFLVSGEPVDIAVSVHRTMQEC MTAATEQKIPGNCYPVDKVIHQDNIE IPAGL
Phage T7 Gp0.4	-	-	5.75	MSTTNVQYGLTAQTVLFYSDMVRCGF NWSLAMAQLKELYENKAI ALES AE

Strains used for testing of NinH were all derivatives of *E. coli* K12.

Table 2: *E. coli* strains used in testing of NinH

Strain	Description	Fis	NinH
LT447	MG1655 (λ cI857 <i>ind1</i>) monolysogen	Y	Y
LT2230	MG1655 (λ cI857 <i>ind1</i> Δ <i>ninH</i>) monolysogen	Y	N
LT2259	MG1655 (λ cI857 <i>ind1</i>) monolysogen <i>fis</i> <> <i>cat</i>	N	Y
LT2260	MG1655 (λ cI857 <i>ind1</i> Δ <i>ninH</i>) monolysogen <i>fis</i> <> <i>cat</i>	N	N

Cells were grown in sterile Luria-Bertani (LB) broth (Sigma-Aldrich) with shaking at 150 rpm (Stuart SI500 Orbital Shaker) or on LB agar and incubated at either 30°C or 37°C. *Kil* strains were supplemented with ampicillin (100 μ g/ml; Melford) or kanamycin (50 μ g/ml; Sigma-Aldrich) as required. Expression of *kil* from plasmid constructs was induced with 1 mM isopropyl β -D-thiogalactoside (IPTG; Melford) and 0.2% L-arabinose (Ara; Melford). For NinH experiments, LT strains were cultivated at 30°C and prophages induced by incubating cells at 42°C for 30 min. A Jenway 6300 Spectrophotometer was used to monitor bacterial growth with optical density readings at 600 nm.

Fresh stocks of all strains on LB agar (with antibiotic as required) were stored at 4°C for 1-2 weeks. Liquid overnight cultures were created by inoculating a single colony from these plates into 5 ml LB (with antibiotic as required) and incubated overnight at 30°C or 37°C. Stocks were refreshed using a sterile plastic inoculation loop to streak overnight culture onto a fresh sterile LB agar plate.

2.2 Bacterial viability assays

A 25 µl sample from an overnight culture was used to inoculate 1 ml of LB broth containing the appropriate antibiotic and grown to an OD_{600nm} of 0.4 at 37°C with shaking (150 rpm). Serial (10-fold) dilutions from 10⁻¹ to 10⁻⁵ were performed and 10 µl aliquots from 10⁻¹-10⁻⁵ were applied to the surface of LB agar plates supplemented with antibiotic and with or without addition of 1 mM IPTG and 0.2% Ara. Plates were incubated for 16-24 hrs at 30°C. Bacterial viability was determined in colony forming units (CFU) per ml with colonies counted manually. Experiments were performed in biological triplicate. Plates were imaged with a Bio-Rad GelDoc Imaging System.

2.3 Protein overexpression

Small scale overexpression from *kil* plasmid constructs in BL21-AI was induced by growing a culture (1 ml from an overnight culture in 7 ml LB supplemented with antibiotic) to an OD_{600nm} of 0.5. The culture was split into two 4 ml volumes in a 15 ml Flacon tube (Sarstedt). Gene expression was induced in one of the cultures by addition of 1 mM IPTG and 0.2% Ara and incubated at 37°C with shaking for a further 2-3 hrs. A 1 ml sample was removed from the uninduced and induced cultures and cells pelleted by centrifugation in a MSE Microcentaur microcentrifuge at 6000 rpm for 2 min. The supernatant was discarded and the pellet resuspended in 150 µl His-Wash Buffer (HWB; 50 mM Tris-HCl pH 7-8, 0.3 M NaCl, 10 mM imidazole).

Samples were prepared for SDS-PAGE analysis by addition of 4 μ l SDS-PAGE loading dye followed by incubation at 90°C for 5 min in a Techne Dri-Block DB.20. Samples were stored at -20°C until ready for separation of total cellular proteins by SDS-PAGE.

Large-scale overexpression was achieved by inoculation of 40 ml LB broth supplemented with antibiotic with 4 ml of a fresh overnight culture. This was used as an inoculum into 500 ml LB broth supplemented with antibiotic in 1 litre baffled conical flasks (to ensure good aeration) and incubated at 37°C, 150 rpm, to an OD_{600nm} of 0.5. Inducers (IPTG and Ara) were added and the flasks incubated for ~2 hours with continuous shaking. Strains carrying the Mu Kil construct were incubated overnight with inducers due to poor growth rate. Cells were harvested in 500 ml vessels using a JA8.1000 rotor in a floor standing centrifuge (Beckman) for 30 min at 4000 rpm at 4°C. The supernatant was discarded and the cell pellet resuspended in 10 ml HWB. The suspension was split into two 15 ml Falcon tubes and stored at -80°C.

2.4 SDS-PAGE

To check protein expression levels, samples were applied and separated on SDS polyacrylamide gels. Pre-poured Mini-PROTEAN TGX Gels 8-16% (Bio Rad) were used to assist in visualising the small proteins involved. Gels were assembled in a Bio-Rad gel tank with running buffer (0.025 M Tris, 0.192 M glycine, 0.01% SDS) added to top and bottom reservoirs. PageRuler™ Prestained Protein Ladder (5 μ l), 10-180 kDa (Thermo Fisher Scientific), was used as a marker loaded in the first well, followed by 10-15 μ l of protein samples in subsequent wells. After loading, the gels were run at 150 V (Consort E132 Power Pack) until the dye front reached the bottom. Gels were stained with Coomassie blue (InstantBlue Coomassie Protein Stain) for ~1 hr with

gentle agitation on a rocking platform. Gels were destained in deionised water overnight and imaged using a Bio-Rad GelDoc Imaging System.

2.5 Protein purification

Cell suspensions from large-scale overexpression were thawed and kept on ice. Once fully thawed the cells were disrupted by sonication (HD 2200 Bandelin Sonopuls) in 10 x 15 s bursts with 30 s gaps. Samples were kept in a water-ice mixture to prevent localised heating. The lysate was centrifuged at 13,000 rpm using a JA25.50 rotor for 30 min at 4°C to remove insoluble proteins and cell debris. The supernatant was transferred to 15 ml Falcon tubes, with 50 µl supernatant set aside for SDS-PAGE analysis. A small portion of the pellet was resuspended in 100 µl of HWB and also prepared for SDS-PAGE analysis, the rest was stored at 4°C.

Nickel affinity chromatography was performed manually using Bio-Rad Poly-Prep chromatography columns set up on a rack. Sufficient nickel-sepharose FF resin suspension (Fujifilm-Diosynth) was added to obtain a 1 ml column. The column was kept topped up with HWB and capped until ready for use. The column equilibrated with 5 ml of HWB and the supernatant from the lysate applied and allowed to flow through. This flow through (FT) was collected and checked on SDS-PAGE to identify any unbound proteins. The column was washed with 5 ml HWB before addition of 10 ml of His Elute Buffer (HEB; 50 mM Tris-HCl pH 7-8, 0.3 M NaCl, 250 mM imidazole) and allowed to run through the column by gravity with ~1 ml fractions collected in 6 x 1.5 ml Eppendorf tubes. Samples were stored at 4°C. SDS-PAGE analysis was performed with samples from; the uninduced and induced overexpression steps, both the pellet and supernatant following lysis, FT and elute fractions (1-6). These samples were prepared and run on SDS gels to identify bound proteins and assess purity.

To check the pellet after lysis for desired proteins, 1 ml HWB containing 8 M urea was mixed with the pellet to denature and resolubilise proteins. Pellet suspensions prepared in this manner were mixed for 4 h on a rotator (Labinco LB79 Rotator) in a cold room at 4°C. These samples were then pelleted by centrifugation at 13,000 rpm for 15 min at 4°C. The resulting supernatant was applied to a 1 ml nickel-sepharose column with inclusion of 8 M urea in all buffers.

2.6 Protein dialysis

To concentrate the protein after chromatography, selected elute fractions underwent buffer exchange using dialysis. Dialysis tubing (Medicell International Ltd., size 2-18/32") was cut to appropriate lengths for pooled elute fractions and placed in a Duran bottle containing deionised water to rehydrate for 2-5 min. Tubing was then washed inside and out with deionised water. One end of the tube was tied and clipped, the elute fractions pipetted in from the open end and the tubing clipped and knotted. Tubing was placed in 1 L of Buffer A (20 mM Tris.HCl, 1 mM EDTA, 0.3 mM dithiothreitol) containing 50% glycerol and 1 M NaCl for 3-4 h with gentle mixing on a magnetic stirrer. Dialysis tubes were then placed into two more buffers, with decreasing NaCl concentrations (0.8 M and 0.6 M), for ~3-4 h each. To recover protein samples, the dialysis tubing was removed from buffers and cut open with recovered samples stored in 1 ml aliquots in 1.5 ml screw-capped Eppendorf tubes stored at -80°C. SDS-PAGE was performed to confirm the presence and purity of protein samples.

2.7 Size exclusion chromatography

Protein sample concentration was determined using a NanoDrop at $A_{280\text{nm}}$.

1 L of HEPES buffer (50 mM HEPES/NaOH, 300 mM KCl, pH 7.5) was filtered and degassed. Samples were run loaded on a Superdex200 column, 10/300GL and run in

HEPES buffer using an AKTA pure system. Flow rate was set to 0.75 ml/min and 0.5 ml fractions collected.

2.8 Bioinformatics analysis

Modelling of Kil proteins, FtsZ and NinH used AlphaFold2 Colab ([AlphaFold2.ipynb - Colaboratory \(google.com\)](#)) (Jumper et al., 2021; Mirdita et al., 2022). Single protein sequences were entered for the construction of Kil proteins and FtsZ monomers. For modelling Kil proteins with FtsZ, each Kil protein sequence was run with the FtsZ sequence separated by a `:`. Models were subsequently analysed in PyMOL (The PyMOL Molecular Graphics System). Kil protein 3D-structures predicted by AlphaFold were compared with known protein structures and each other using the DALI server ([Dali server \(helsinki.fi\)](#)) (Holm et al., 2023).

2.9 Microscopy

Overnight cultures (100 μ l) were added to 2 ml LB broth and grown in a shaking incubator at 37°C to an OD_{600nm} of 0.3. The culture was split into two 1 ml samples in 1.5 ml Eppendorf tubes and placed on ice. One of the tubes was incubated for 30 min at 30°C, slides were prepared and imaged. The other tube was incubated for 30 min at 42°C, slides were prepared and imaged. The 42°C heat treatment will induce the λ prophage to enter the lytic phase as a result of the temperature sensitive *ci857* allele. Samples (250 μ l) were transferred to fresh Eppendorf tubes and cells pelleted by centrifugation for ~5 min at 5000 rpm. The supernatant was discarded and cell pellet resuspended in 100 μ l DAPI (10 μ l triton x100, PBS, DAPI). A 10 μ l sample of the resuspended pellet was transferred onto a glass microscope slide, covered and sealed with clear nail varnish.

All samples were imaged using a Leica SP5 II LSCM microscope coupled to Leica Application Suite Advanced Fluorescence imaging software. Image processing and data extraction was performed using Fiji.

3. Results

This study aims to further characterise Kil proteins and NinH with relevance to their potential as novel phage antibacterials. To achieve this, seven Kil proteins were selected (Table 1) for testing. Unfortunately, T7 Gp0.4 could not be tested *in vitro* due to excessive toxicity, causing loss of *E. coli* viability even in cells without induction of expression from the plasmid construct. The T7 Gp0.4 structure was still investigated using computer modelling approaches. To assess NinH effects, four prophage constructs with or without deletion of the *ninH* gene (Table 2) were tested in microscopy experiments.

3.1 Antibacterial activity of Kil proteins

To determine the effect of the selected phage and prophage Kil proteins on *E. coli* growth and viability, toxicity assays were performed (Figure 7). *E. coli* BL21-AI strains carrying each of the *kil* genes in a pET vector were examined under uninduced and induced conditions on LB agar plates. Selective expression of the Kil proteins was achieved by addition of 0.2% L-arabinose and 1 mM IPTG to activate the phage T7 promoter in each construct.

In the uninduced plates, there was no significant difference in the growth or viability of λ Kil relative to its vector control pET22b (Figure 7). Similarly, Rac Kil, P22 Kil and YdfD all showed no significant difference in colony size or number compared to pET28a in the absence of induction. In contrast, Mu Kil and DicB both showed a reduction in viability compared to the relevant pET28a control without addition of inducers with log fold reductions of 1.82 and 0.88, respectively (Figure 8). These results suggest that even low level ‘leaky’ expression of these two Kil proteins is toxic to *E. coli*.

Under induced conditions, λ Kil expression resulted in a log 1.68-fold reduction in *E. coli* viability (Figure 7 and 8). There was some variability in the extent of toxicity, with several plates showing no colonies at 10^{-2} while others retained colonies at 10^{-4} (Figure 7).

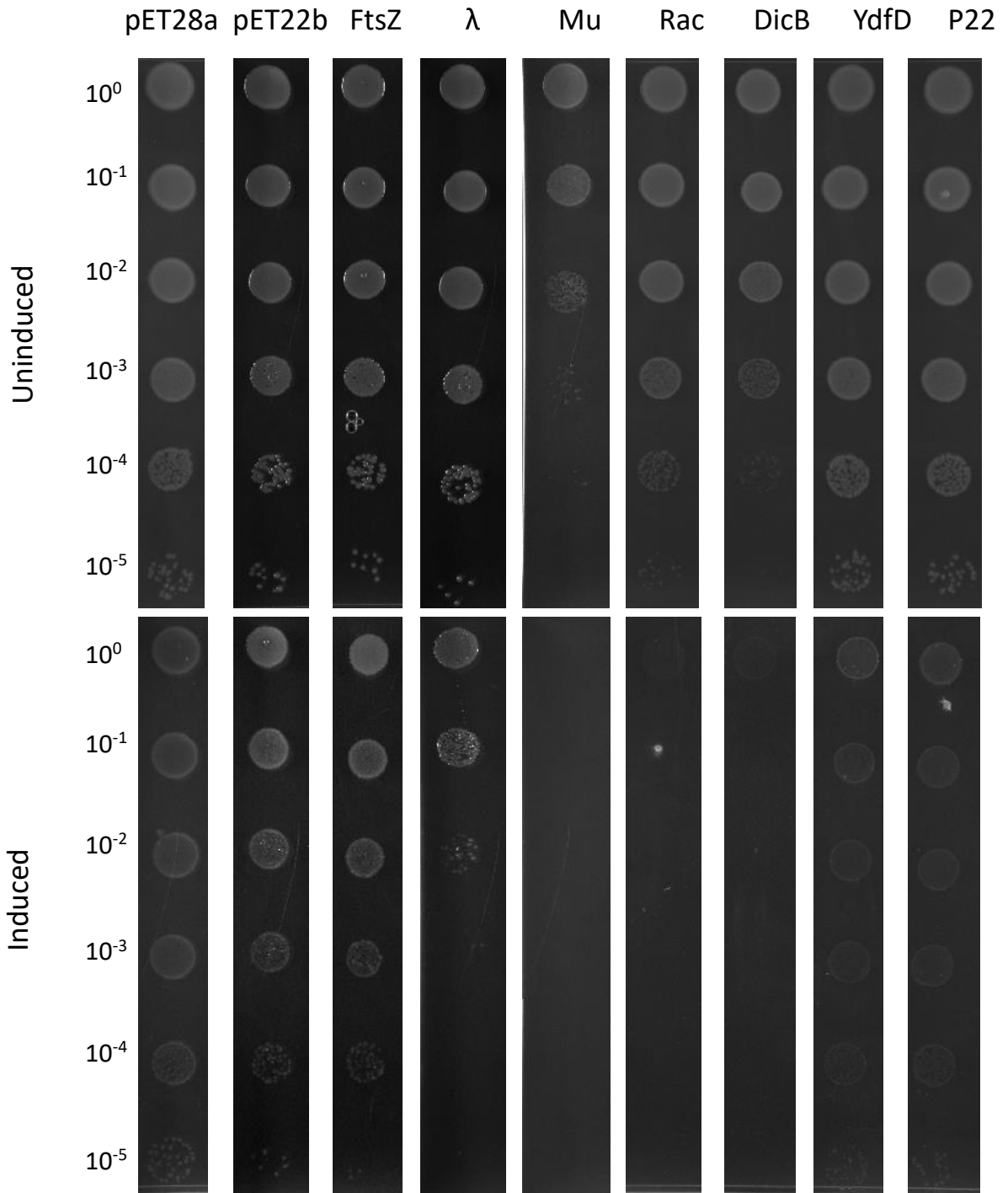


Figure 7: Bacterial viability assays of transformed BL21-AI. Strains labelled along the top, y-axis shows the culture dilutions. Top, uninduced agar plates + antibiotic. Bottom, induced agar plates + antibiotic + 1mM IPTG + 0.2% L-Arabinose.

Mu Kil, Rac Kil and DicB showed more substantial reductions in viability of log 2.24-, 4.85- and 4.39-fold, respectively (Figure 8). Mu Kil in all but two cases completely eliminated colony formation at all dilutions (Figure 7). In the two exceptions, a small number of colonies was noted at the 10⁻¹ dilution, which is still a significant difference between the control and uninduced plates. Across all repeats, Rac Kil expression led to colonies forming only in the undiluted sample, with the highest count at 29 and an average of only 7 colonies. DicB exhibited a similar effect with no colonies except in the undiluted sample, with its highest count at 11 and an average of 4 colonies.

Following application on plates containing arabinose and IPTG, neither YdfD nor P22 exerted any deleterious effect on *E. coli* viability (Figure 7 and 8). However, in both cases there was a marked reduction in colony size consistent with some impact on bacterial growth.

E. coli Colony Count before and after Induction of Phage Peptides

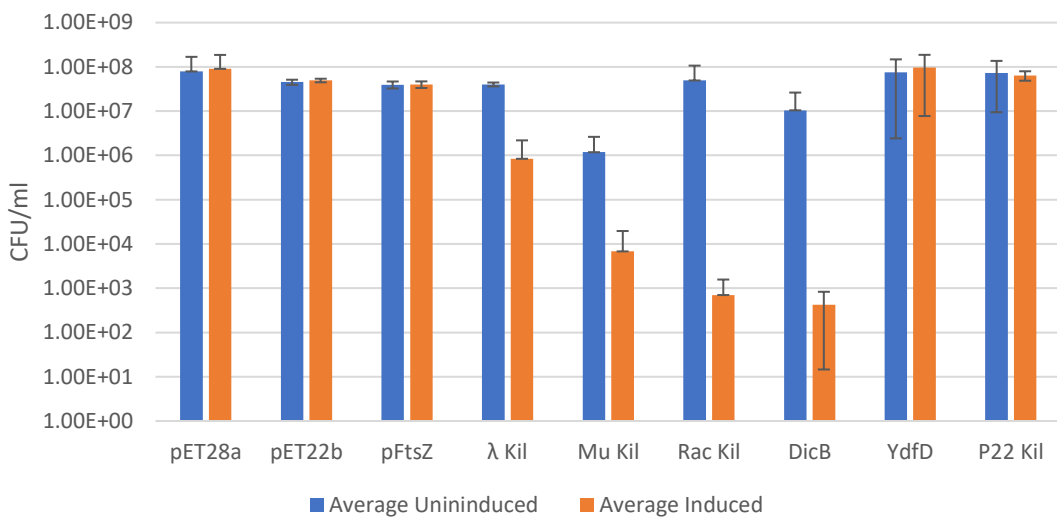


Figure 8: *E. coli* viability following expression of phage polypeptides. y-axis colony forming units (CFU) per millilitre, x-axis strain labels. Bacteria carrying constructs expressing phage genes were cultivated in LB media and diluted cultures applied to LB agar plates with and without addition of IPTG and arabinose. Results are the mean and standard deviation of independent experiments performed in triplicate.

Overall, λ Kil, Mu Kil, Rac Kil and DicB caused a significant reduction in *E. coli* viability. Mu Kil, Rac Kil and DicB all proved more toxic than λ Kil (Figure 8). Rac Kil proved the most toxic (Figure 7), likely entirely killing all *E. coli* cells, while Mu Kil and DicB also had significant detrimental effects on viability even in the absence of inducers. The variation in apparent toxicity could have been caused by rapid plasmid loss or potentially the development of resistance. Slow growth of *E. coli* carrying the Mu Kil plasmid was apparent, requiring an additional hour of incubation to reach an OD₆₀₀ 0.4 compared to the other plasmid-bearing strains. Although YdfD and P22 did not reduce viability, there was a reduction in colony size consistent with some effect on bacterial growth.

3.2 Protein overexpression

To further investigate the toxicity of Kil proteins in *E. coli*, we attempted to overexpress and purify the proteins for biochemical characterisation. Firstly, the proteins were overexpressed on a small scale (5 ml) and samples separated by SDS-PAGE to confirm successful overproduction of each protein (Figure 9).

The gel analysis confirmed the presence of Rac Kil with a strong band at ~12 kDa present under induced conditions and corresponding to the expected mass of 10.59 kDa. High-level overexpression of YdfD, P22 and λ Kil was confirmed with bands of 10-15 kDa, and the presence of a faint band of a similar size with DicB (Figure 9). Despite these values being larger than their expected molecular mass, it is likely that these bands do correspond to the Kil proteins as they were not present under uninduced conditions. In contrast, there was no apparent induction of Mu Kil. This is likely due to the toxicity of Mu Kil and the challenge of culturing these cells in large quantities, as evidenced by the reduced total cellular proteins present in these samples (Figure 9).

Overproduction of *E. coli* FtsZ was attempted but no band of the appropriate size (40 kDa) was evident in induced samples (Figure 9).

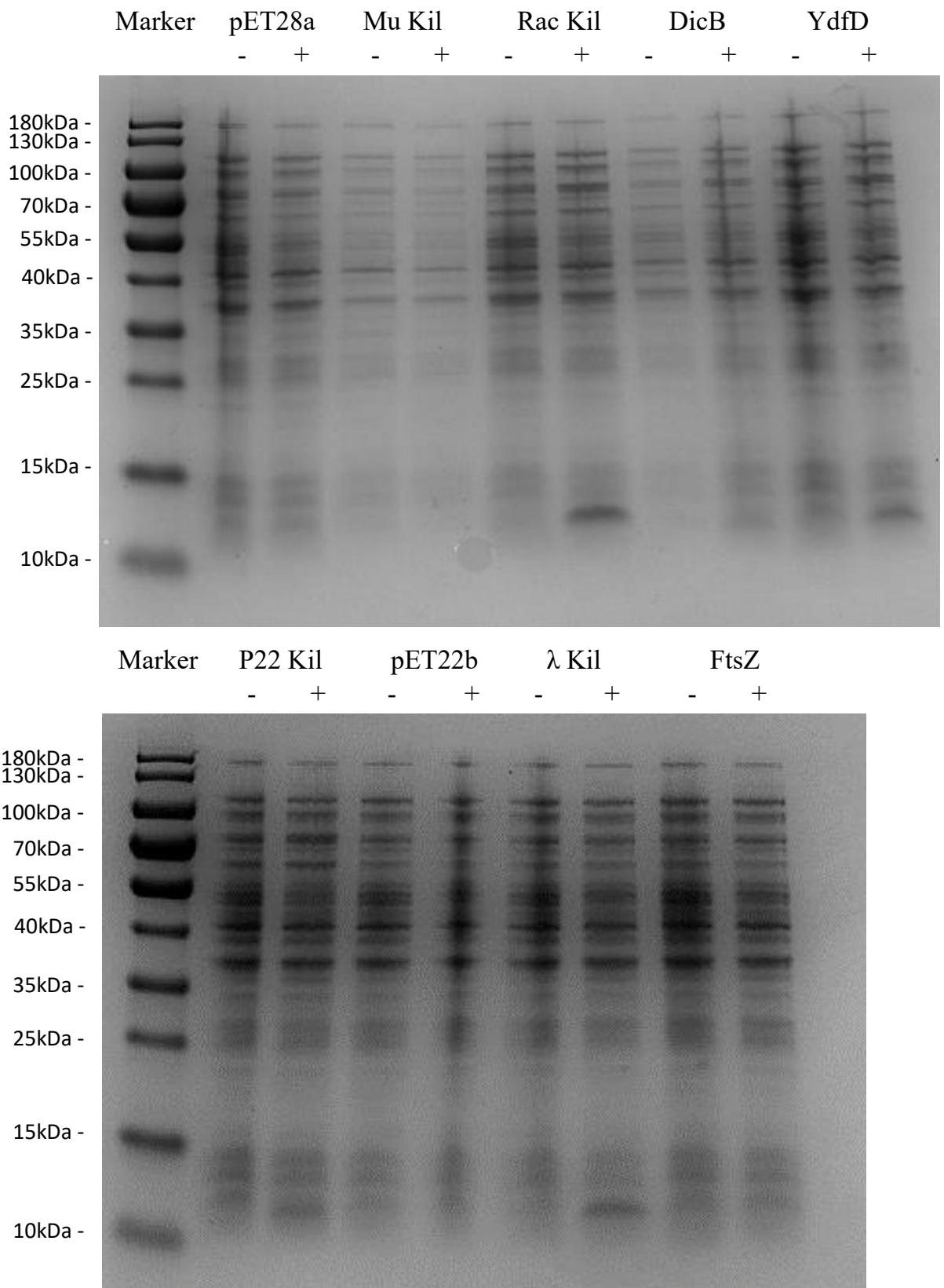


Figure 9: 8-16% gradient polyacrylamide gels showing small-scale overexpression of uninduced (-) and induced (+) Kil proteins. Gels were stained in Coomassie Brilliant Blue.

3.3 Protein purification

Based on the information gained from the small-scale overexpression experiments, larger volumes (500 ml) were grown to produce sufficient λ Kil, Mu Kil, Rac Kil, DicB, YdfD and P22 Kil proteins for purification by nickel-affinity chromatography. Mu Kil, P22 Kil and YdfD were tentatively identified in fractions from the column eluted by the addition of buffer containing imidazole (Figure 10). However, these candidate proteins were contaminated by other cellular proteins and may not be the desired Kil products. Similarly, Rac Kil and DicB may be present in the second elute fraction, but again were not separated from the other contaminating proteins (Figure 10). λ Kil does not appear to be present in the elute. In all six cases there was a large amount of protein of the correct molecular mass in the insoluble, pellet fraction after lysis and there was a strong likelihood that the bulk of the overexpressed Kil protein was located here following lysis.

To obtain purified Kil proteins, the pellet fraction was exposed to 8M urea to denature and resolubilise the proteins for subsequent purification. The resolubilised samples were applied to nickel sepharose columns as before, but with all buffers containing 8M urea to maintain the proteins in a soluble state. SDS-PAGE analysis (Figure 11) indicated bands of the expected molecular mass for λ Kil, Mu Kil, Rac Kil, YdfD and P22 Kil all of which have been purified to varying degrees of homogeneity. Rac Kil yielded the greatest amount of purified protein. Purification was unsuccessful with DicB (Figure 11) and it is possible that the bulk of the protein was actually present in the supernatant but bound poorly to the nickel Sepharose (Figure 10). This poor binding could be due to the His-tag on DicB being embedded in the protein and therefore the His-Tag would have been unable to contact and bind to the resin.

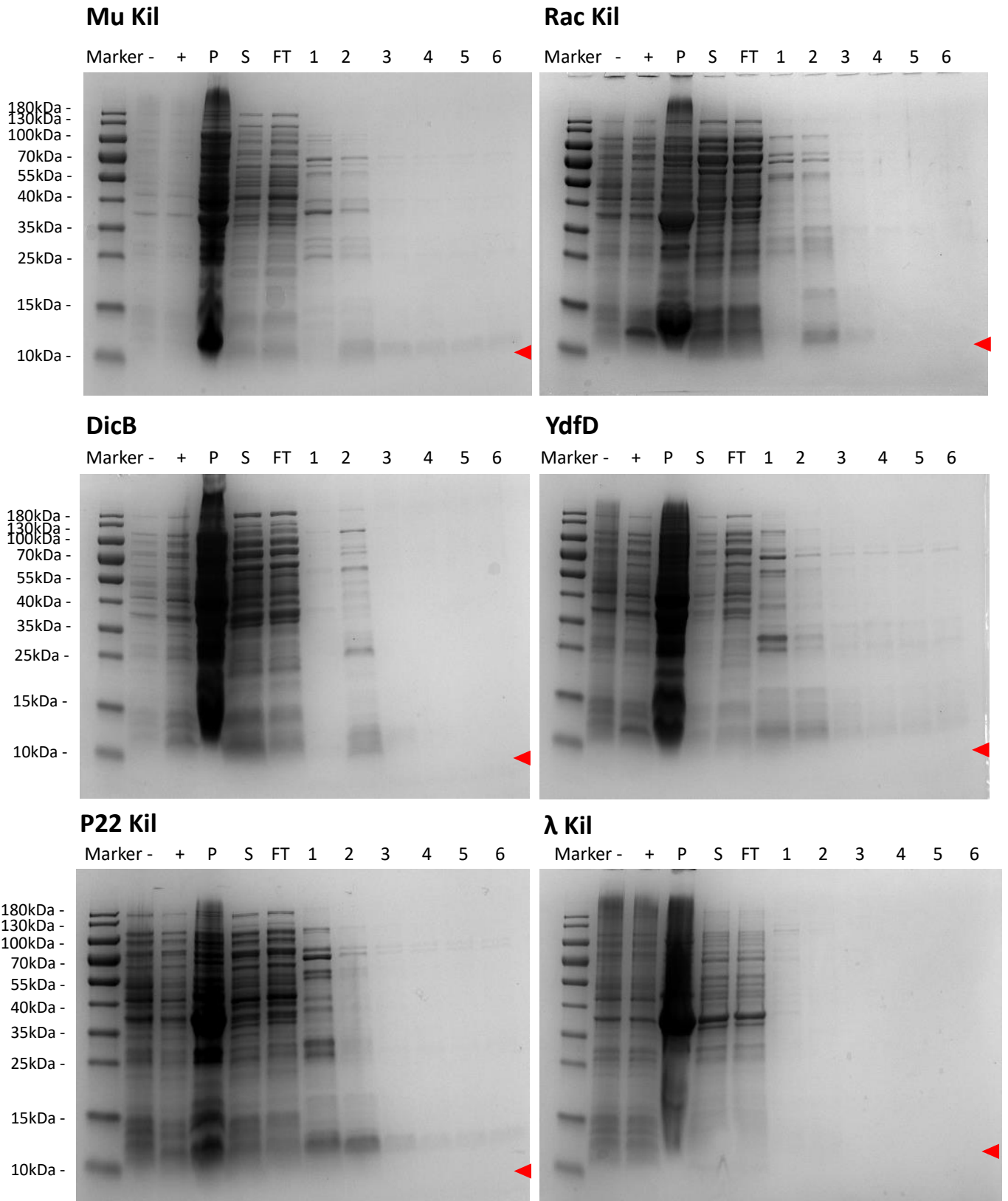


Figure 10: 8-16% SDS-PAGE of KIL proteins isolated by nickel-affinity chromatography stained by Coomassie Brilliant Blue. Uninduced (-) and induced (+) *E. coli* BL21-AI carrying plasmids expressing KIL proteins were lysed and pellet (P) and supernatant (S) separated. The flow through (FT) from the nickel-sepharose column was collected and fractions (1-6) collected following elution. Red arrows indicate expected molecular weight.

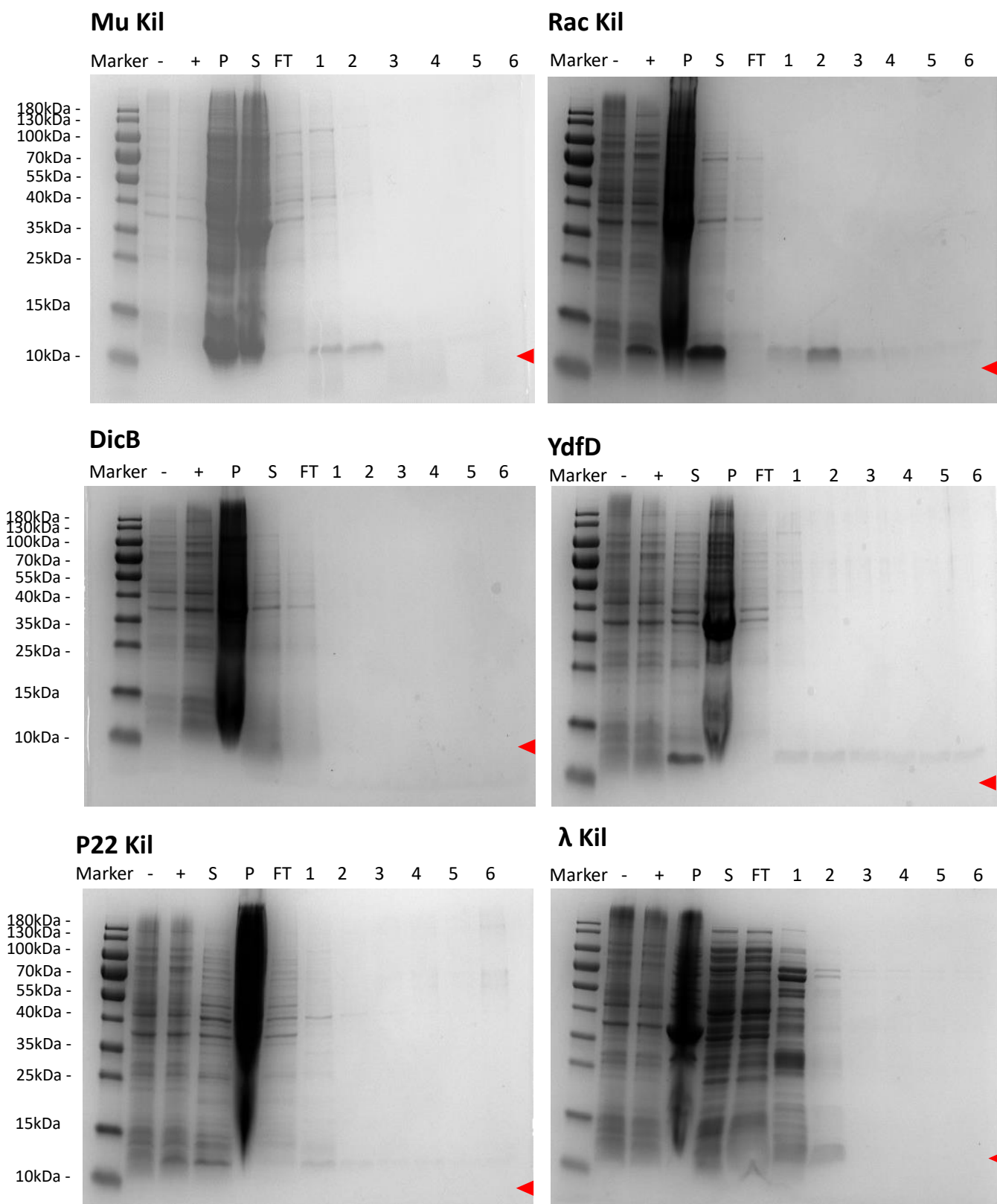


Figure 11: 8-16% SDS-PAGE of Kil proteins purified by nickel-affinity chromatography after denaturation with urea. Stained by Coomassie Brilliant Blue. Uninduced (-) and induced (+) *E. coli* BL21-AI carrying plasmids expressing Kil proteins were lysed and pellet (P) and supernatant (S) separated. The flow through (FT) from the nickel-sepharose column was collected and fractions (1-6) collected following elution. Red arrows indicate expected molecular weight.

The Kil proteins in the eluted fractions were dialysed in a stepwise fashion against buffer containing 50% glycerol and high salt concentrations to aid refolding of the proteins from their denatured state. This proved successful and each of the Kil proteins

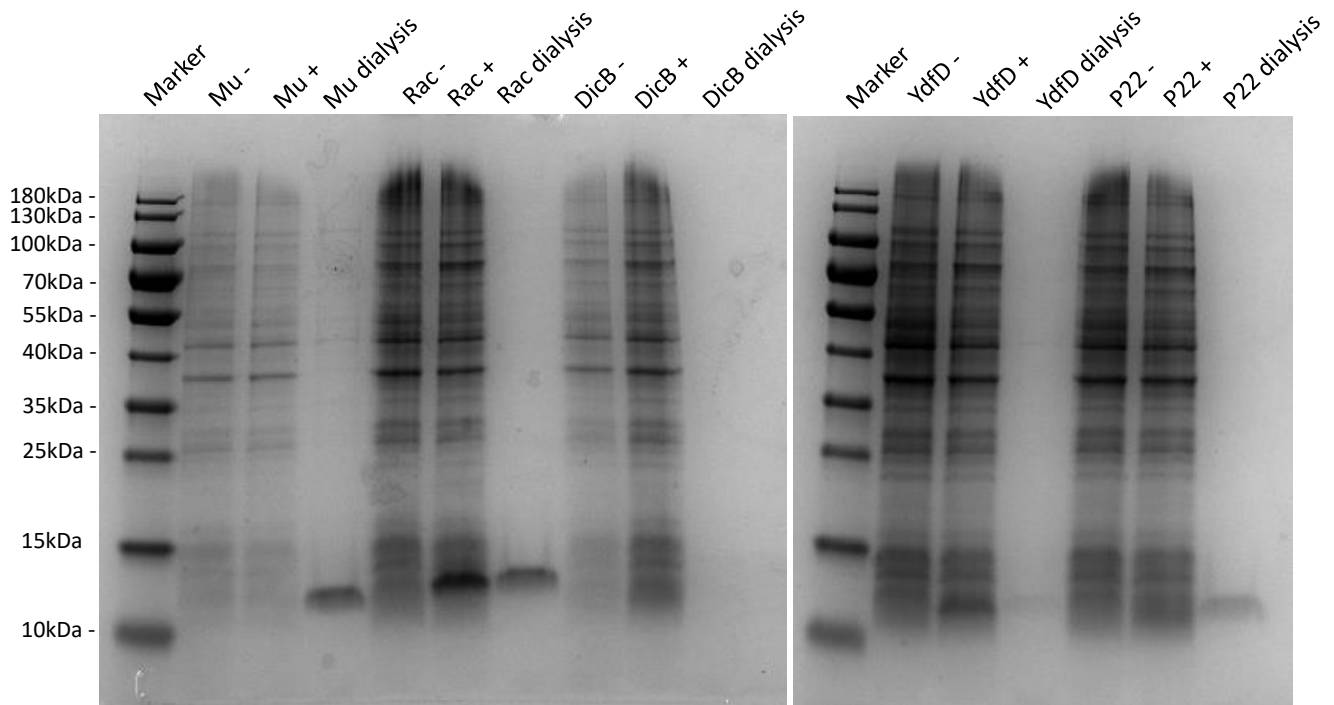


Figure 12: 8-16% SDS-PAGE of purified and dialysed Kil proteins stained with Coomassie Brilliant Blue. Uninduced (-) and induced (+) *E. coli* BL21-AI carrying plasmids expressing Kil proteins.

remained in solution in concentrated form. SDS-PAGE of the dialysed proteins (Figure 12) revealed clear bands between 10 and 15 kDa for all proteins apart from DicB and λ Kil (result not shown). There was much less YdfD recovered, however, all other proteins showed good levels of purity (Figure 12). Protein concentration measurements confirmed Rac Kil as having the highest amount recovered, closely followed by Mu Kil, although this sample contains several higher molecular mass contaminants (Table 3). Although not visible in SDS polyacrylamide gels, small quantities of DicB may be present in this dialysed sample (Table 3).

Table 3: Kil Protein concentrations in samples after dialysis.

Kil Protein	Concentration (mg/ml)
Mu Kil	0.344
Rac Kil	0.307
DicB	0.122
YdfD	0.075
P22 Kil	0.244

3.4 Protein:protein interaction assay

Size exclusion chromatography was employed to assess whether any of these Kil proteins interact with FtsZ (Figure 13). *E. coli* N-His-FtsZ had been purified in a previous project using nickel affinity chromatography. Rac Kil was selected as the most concentrated sample with the best purity. FtsZ and Rac Kil were first applied to a gel filtration column separately, before the mixture of the two was examined. The peak for Rac Kil corresponded well to its molecular mass as a monomeric species. FtsZ, however, appeared as several broad peaks, which could indicate a low quality or deteriorating sample. It is perhaps more likely that the FtsZ has oligomerised to yield a range of multimers of different molecular mass (Figure 13). When Rac Kil and FtsZ were mixed together, several more discrete peaks were observed. It is possible that there was some interaction between the monomeric Rac Kil and the FtsZ although it was difficult to distinguish such an interaction due to the number of peaks observed (Figure 13).

SDS-PAGE analysis of the fractions eluting from the column was inconclusive as the protein samples were too diluted by this stage to be visualised. The lack of a single discrete peak with FtsZ on the gel filtration column and the inability to detect protein

bands by SDS-PAGE, resulted in the decision not to attempt a similar analysis with the other, less concentrated, Kil protein samples.

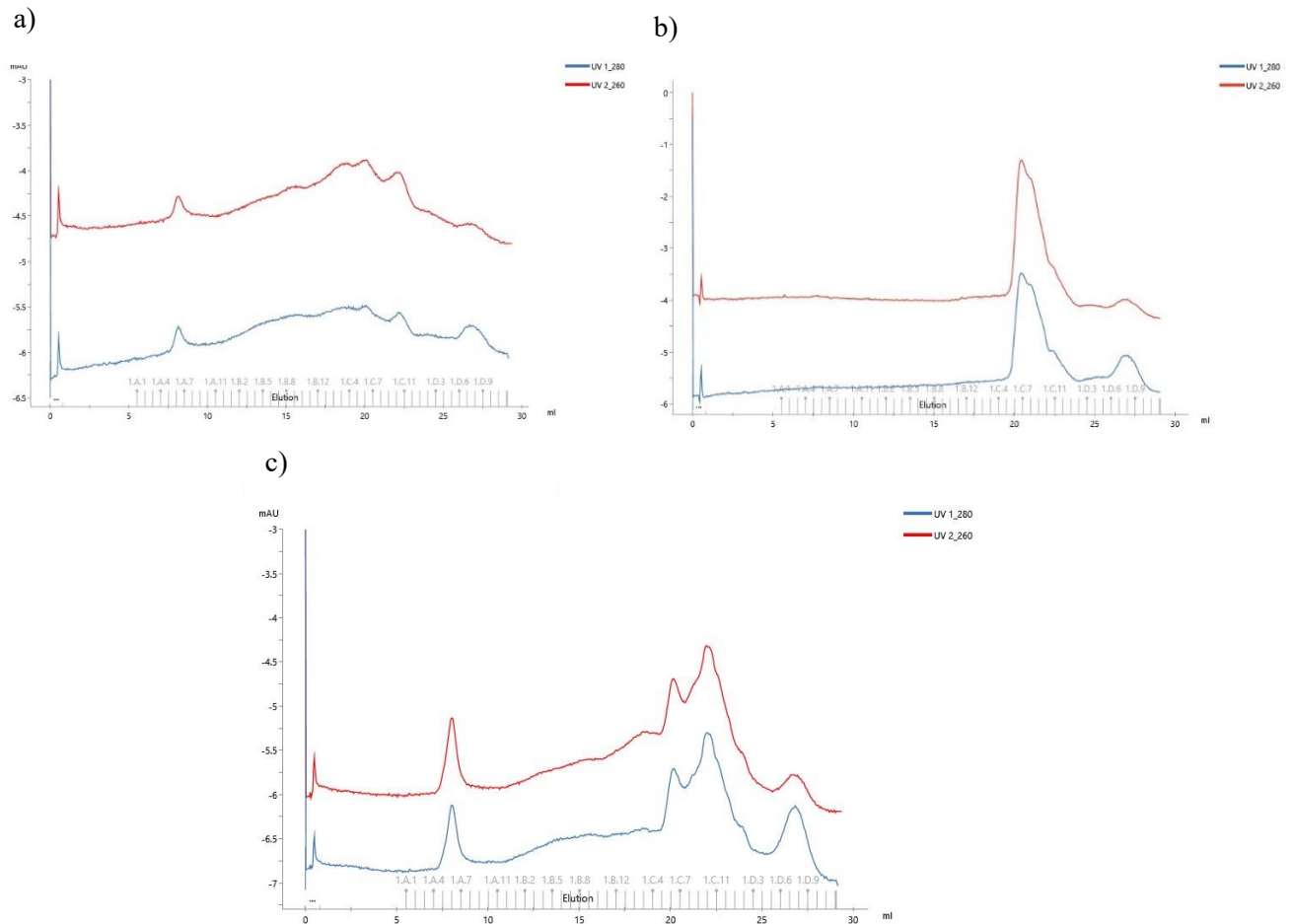


Figure 13: Size exclusion chromatography graphs. a) FtsZ b) Rac Kil c) FtsZ+Rac. FtsZ has a broad peak over multiple elutions. Rac Kil has a sharper peak indicative of a small protein of the expected molecular weight. FtsZ + Rac Kil has a broad peak again but with several discrete peaks however it cannot be distinguished if there has been an interaction between FtsZ and Rac Kil.

3.5 AlphaFold models

Following the inconclusive results from the size exclusion chromatography a modelling approach was used to gain further insight into the Kil protein structures and their potential for interaction with FtsZ.

AlphaFold colab was able to predict a structure for each of the Kil proteins. Confidence levels of these structures was based on a per-residue measure of local confidence - predicted local distance difference test (pLDDT), which scales from 0 –

100, a higher score indicates higher confidence and a more accurate prediction (Mariani et al., 2013). A pLDDT above 90 likely indicates that both the backbone and side chains have been predicted with high accuracy. A pLDDT above 70 implies a correct backbone prediction but misplacement of some side chains. AlphaFold models for each Kil protein yielded high confidence (>90%) across the entire length of each polypeptide (Figure 14), with the exception of λ Kil. Mu Kil, P22 Kil and YdfD all

have different combinations of helices and sheets. Rac Kil appears to be the only protein without helices, composed primarily of β -sheets forming a ring like structure. DicB, Gp0.4 and λ Kil all seem to possess a similar ‘U’ shaped structure of 2 helices. The AlphaFold capability to model protein-protein interactions was utilised to predict potential associations between the Kil proteins and *E. coli* FtsZ (Figure 15). These models suggest that only Rac Kil and T7 Gp0.4 are likely to bind directly to FtsZ.

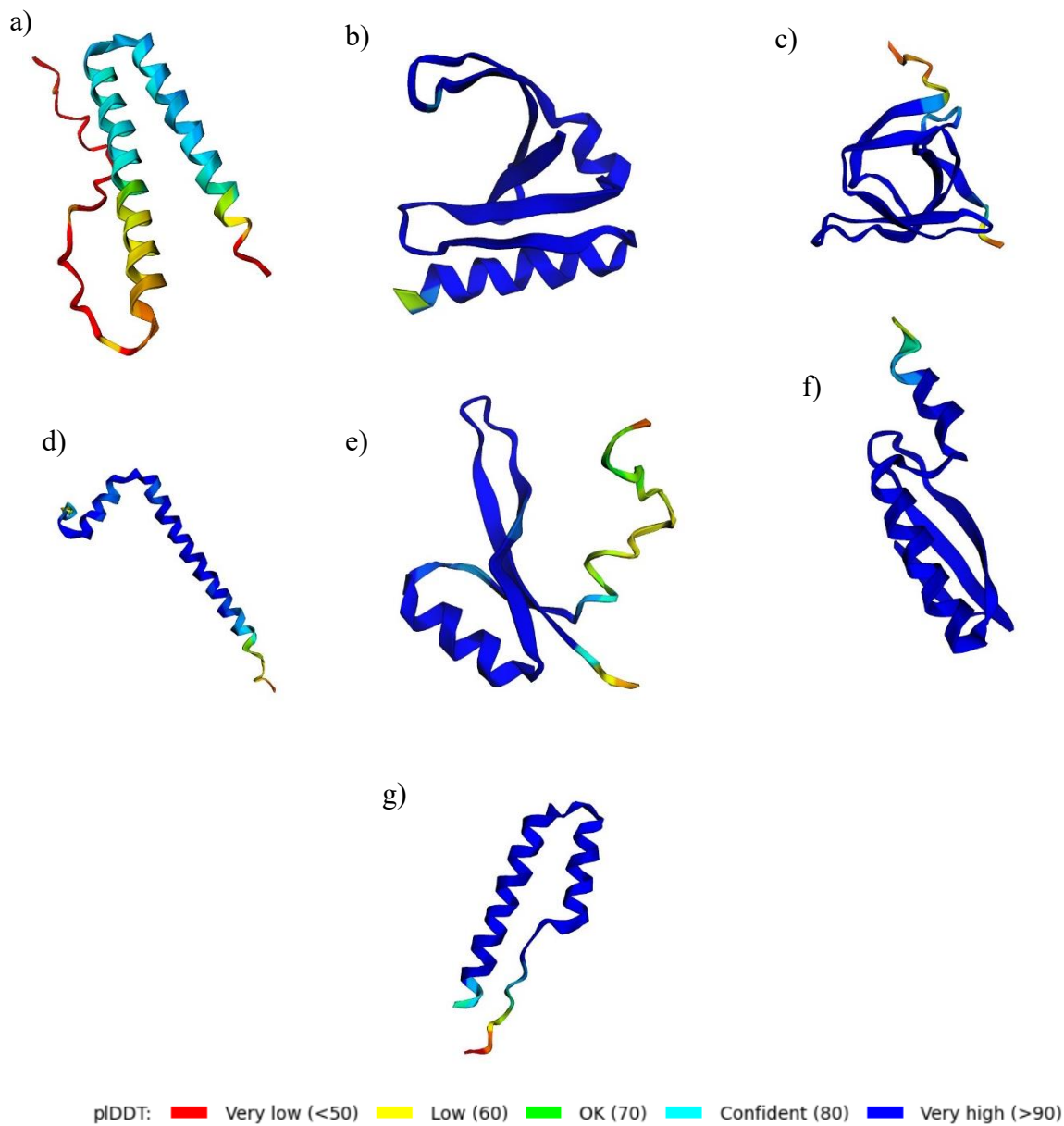
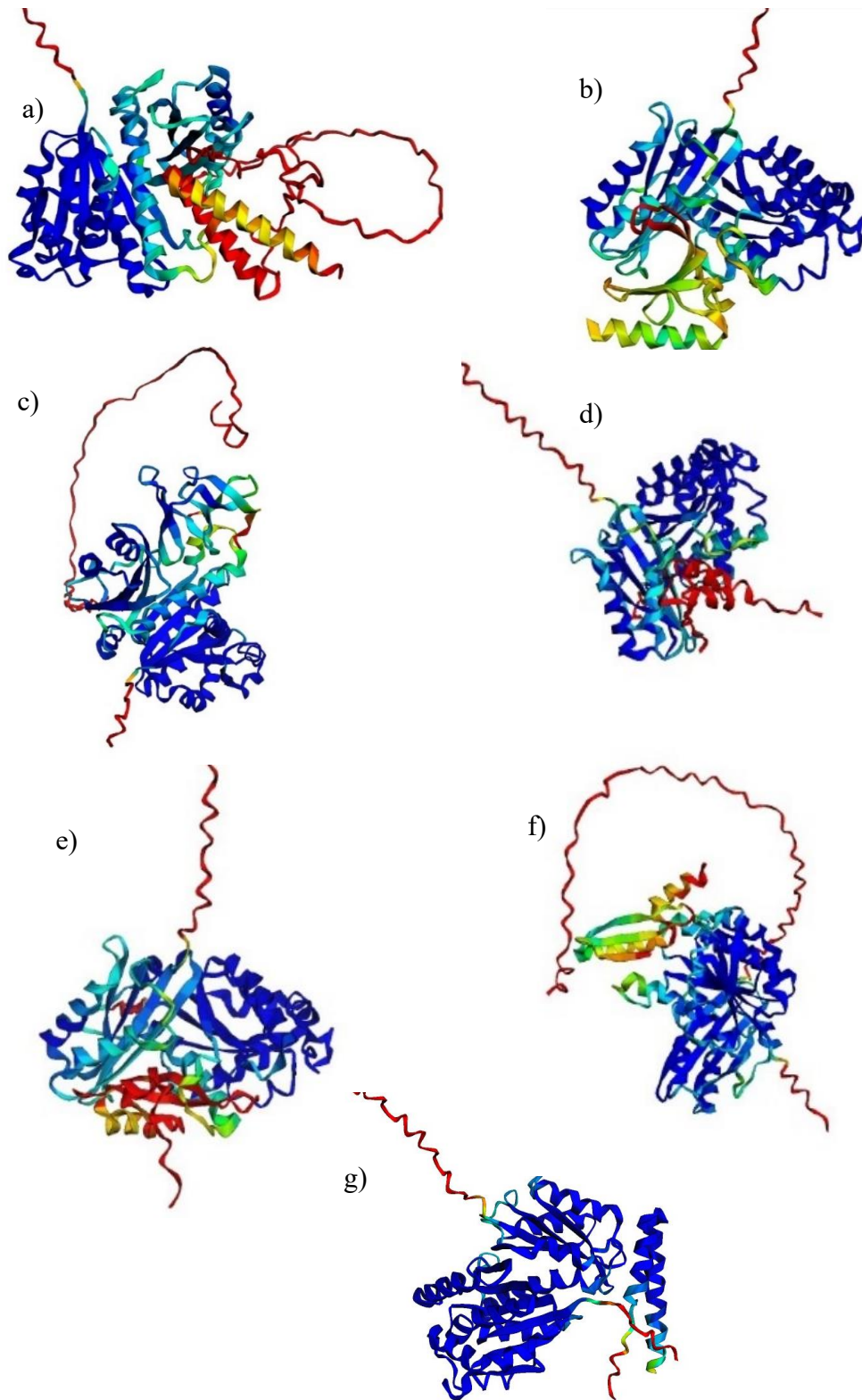


Figure 14: 3D-structural models of Kil proteins produced using AlphaFold2 Colab. Colour on the models corresponds to pLDDT score, indicating confidence in the structure. a) λ Kil, b) Mu Kil, c) Rac Kil, d) DicB, e) YdfD, f) P22 Kil, g) T7 Gp0.4

However, conclusive results cannot be obtained from the pLDDT score alone as this is a measure of local confidence and not always accurate for protein-protein interactions. The predicted aligned error (pAE) plot is a better measure for overall protein alignment (Figure 18). These show the association in the current position to be probable for T7 Gp0.4. Given that λ Kil is known to associate (Hernández-Rocamora et al., 2015), it was surprising that there was not a better match between these two partners. This finding does highlight the limitations of this modelling approach. Mu Kil was potentially able to bind FtsZ, however, as the confidence score across the region of binding was less than 50%, this is unlikely (Figure 15b).



pLDDT: ■ Very low (<50) ■ Low (60) ■ OK (70) ■ Confident (80) ■ Very high (>90)

Figure 15: AlphaFold models of FtsZ and Kil protein interactions. Colour on the models corresponds to pLDDT score, indicating confidence in the structure. a) Lambda Kil, b) Mu Kil, c) Rac Kil, d) DicB, e) YdfD, f) P22 Kil and g) Gp0.4.

The models of λ Kil, Rac Kil, Mu Kil and T7 Gp0.4 bound to FtsZ were examined in more detail (Figure 16). Previous work (Haeusser et al., 2014) has linked *E. coli* FtsZ residues L169 and V208 as important for λ Kil binding and these are highlighted. This

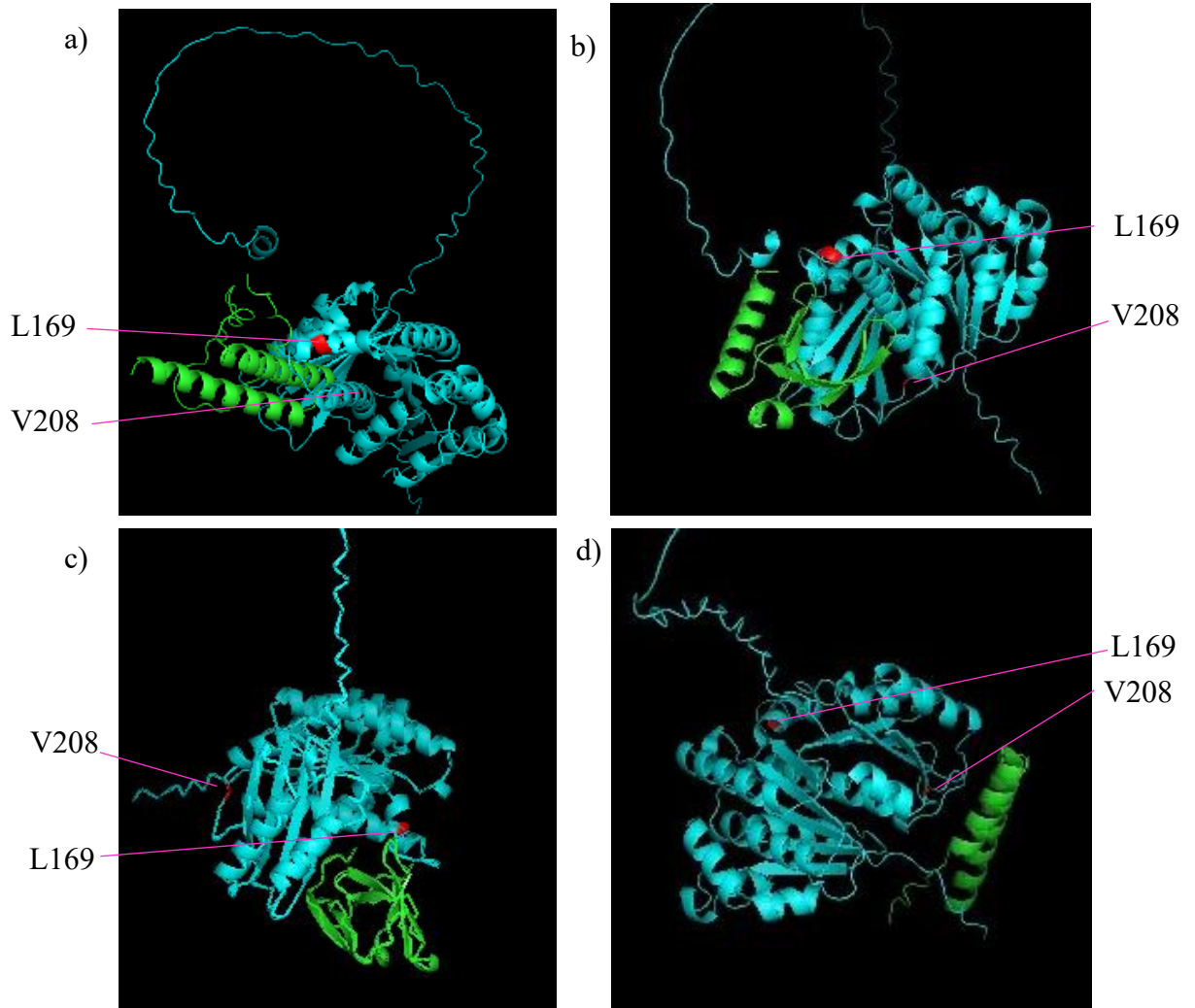


Figure 16: AlphaFold models showing FtsZ (cyan) and Kil protein (green) potential interactions with FtsZ residues L169 and V208 shown in red. Imaged from PyMOL. a) λ Kil, b) Mu Kil, c) Rac Kil, d) T7 Gp0.4

region is responsible for FtsZ multimerization and binding of Kil proteins here would be expected to disrupt FtsZ ring assembly and hence prevent cell division. It can be seen that, despite the low confidence score of the λ Kil-FtsZ complex, the position of contacts between the two proteins is in the appropriate vicinity. Both Mu Kil and Rac Kil share a similar placement around the L169 residue, however T7 Gp0.4, is the only

one to localise closer to V208. Given the differences in structure between these Kil proteins it would not be too surprising if their binding sites on FtsZ also differed.

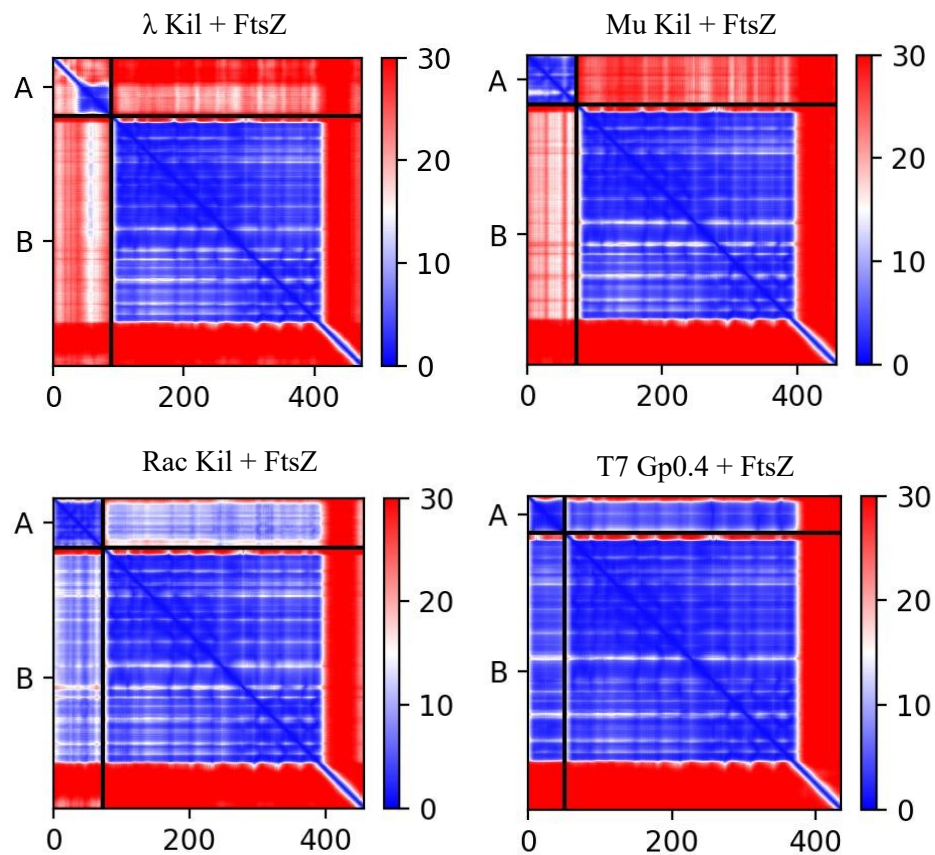


Figure 17: Predicted aligned error (pAE) for the corresponding AlphaFold models. The lower the predicted aligned error the darker shade of blue.

3.6 Kil proteins analysed on the Dali server

Using the Protein Data Bank (PDB) files that were generated by AlphaFold2 Colab, the predicted Kil 3-D models were compared to those of other protein structures in the database using the DALI server. Kil protein structures were also compared against each other and with FtsZ. Results with a Z-score >8 are expected to be indicative of a genuine match. In this search, none of the seven protein searches returned a Z-score of greater than this significance. Rac Kil had the highest Z-score at 7.1, the match was with Eukaryotic Translation Initiation Factor 5A (eif5A). These two proteins share a 12% identity over a region of 134 amino acids. Pairwise structural alignment revealed that despite few matches in amino acid sequence, their secondary structures were

remarkably similar (Figure 18). This could be detrimental in using Rac Kil as an antibacterial if it could interact with eukaryotic proteins and therefore be potentially

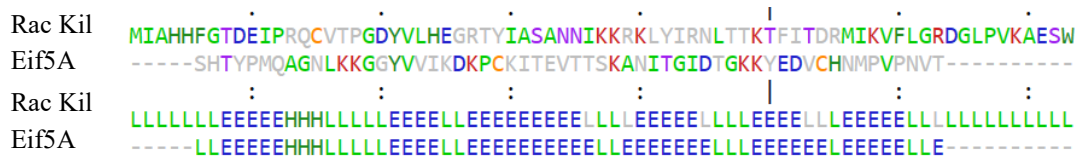


Figure 18: Pairwise structural alignment of Rac Kil and eif5A. Upper block showing amino acid sequence, lower block secondary structure states L = Coil, H = Helix and E = Sheet.

toxic to humans. 3-D superimposition of these two proteins where they overlap was performed by a rigid body transformation in Protein Viewer (PV; Figure 19).

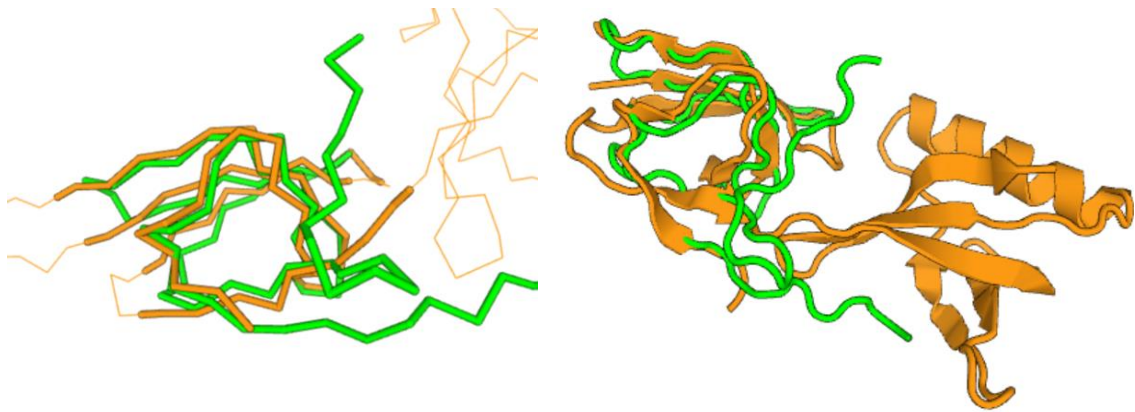


Figure 19: DALI server 3D-superimposition of Rac Kil (green) and eif5A (orange). Structural models from AlphaFold (Rac Kil) and the PDB (eif5A) were used.

A pairwise comparison of the Kil proteins and FtsZ showed no similarity between them ($Z < 0.1$), suggesting that mimicry is not a likely source of any disruption of FtsZ functionality. However, correspondence analysis, which positions data points based on similar structural neighbourhoods, suggested that DicB and T7 Gp0.4 have the most similar 3-D structures (Figure 20). This is in accordance with each forming a long and short alpha-helix hairpin (Figure 15).

Correspondence Analysis

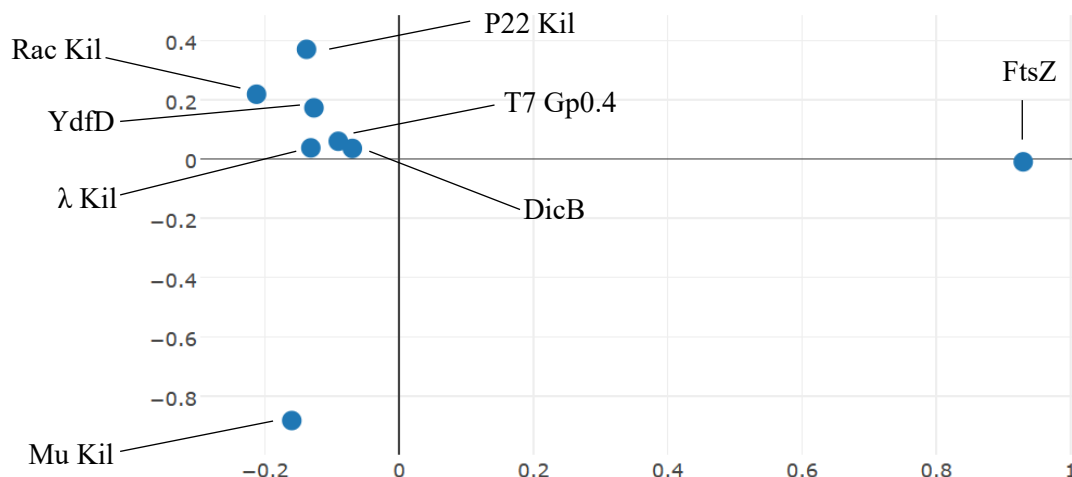


Figure 20: Correspondence analysis taken from DALI server. x and y axes showing similarity through structural neighbourhoods.

3.7 Examination of the *in vivo* role of phage λ NinH

NinH is a small protein, from prophage λ produced exclusively during the lytic cycle. NinH shares sequence similarity to Fis and is a functional homologue. Four strains were tested, each with a combination of NinH and/or Fis knockouts and the relevant control (Table 2). The object of this was to identify the competing cellular targets of NinH and Fis by examining any morphological changes in *E. coli* cells.

Cells were stained with DAPI to visualise chromosomal DNA and imaged with an LSCM microscope. Cell length was measured manually in ImageJ. The λ prophage in each strain was induced by shifting the temperature from 30° to 42°C, resulting in inactivation of the cI allele and pushing the phage into the lytic cycle. *E. coli* strain LT447 (MG1655: λ cI857 *ind1 ninH⁺ fis⁺*) under uninduced conditions grew relatively normally with an average cell length of 2.5 μm (Figure 21b). Under induced conditions, the average cell length increased by 0.5 μm to 3 μm . Furthermore, there

were a greater number of outliers in cell length with the longest imaged being $\sim 21 \mu\text{m}$ (Figure 21b).

LT2230 (MG1655: λ cI857 *ind1* Δ *ninH* *fis*⁺) grew similarly under both induced and uninduced conditions with an average cell length of $2.2 \mu\text{m}$ and $2.4 \mu\text{m}$ (Figure 21b). In comparison to LT447 (*ninH*⁺ *fis*⁺), the average cell length has not increased as much, which could be attributed to the absence of *ninH* in the LT2230 prophage. However, the differences are modest and so no clear conclusions can be drawn.

LT2260 (MG1655: λ cI857 *ind1* Δ *ninH* *fis*::*cat*) produced abnormally long cells. The

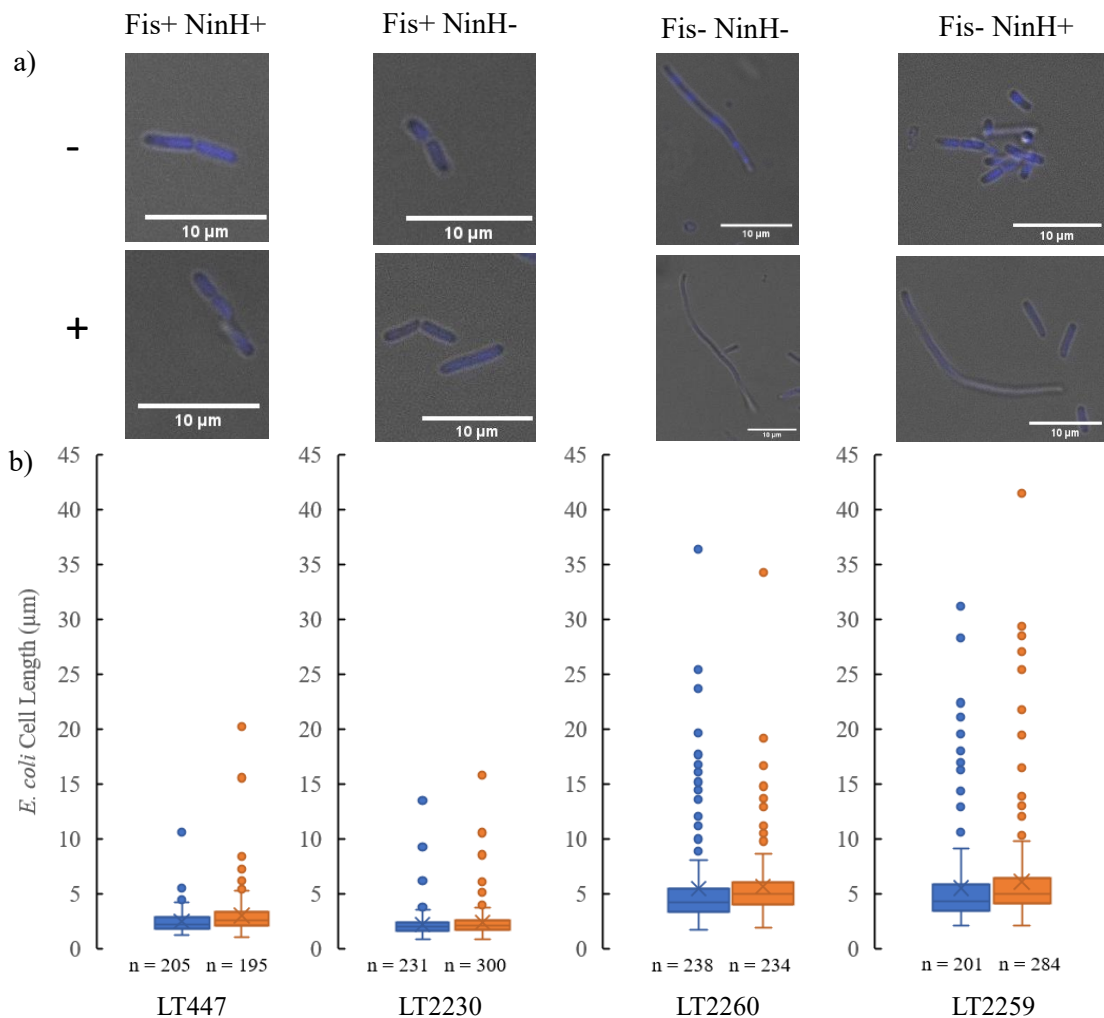


Figure 21: a) Images of uninduced and induced *E. coli* cells for each strain. **b)** Box and whisker plots. Blue = uninduced, Orange = induced. Y-axis showing cell length

average size for uninduced and induced $5.5 \mu\text{m}$ and $5.7 \mu\text{m}$, respectively (Figure 21b),

including many more outliers of greater length being found. The largest cell found was measured 36.4 μm in length. The average cell length is far from normal and is consistent with the absence of *fis* from the bacterial chromosome. There were no significant differences in cell size between uninduced and induced cultures.

LT 2259 (MG1655 λ cI857 *indI ninH⁺ fis::cat*) cells also grew abnormally long, with an average cell size of 5.5 μm and 6.1 μm (Figure 21b) for uninduced and induced cultures, respectively. Again, there were multiple outliers, the longest being ~ 41.5 μm . No significant difference in cell length could be distinguished between the uninduced and induced cells. However, the uninduced cells tended to clump together making it more difficult to manually measure the lengths of the smaller cells, which could have skewed the data.

Wild type *E. coli* cells should be short, rod shaped and nucleated. Cells lacking *fis* are known to filament, have reduced nucleoid size and exhibit aberrant nucleoid segregation (Filutowicz et al., 1992). In this study, the DNA was stained with DAPI. *Fis⁺* cells without induction of the λ prophage showed a normal distribution during division (Figure 22a). In contrast, cells lacking *fis* are abnormally elongated and failed to complete normal chromosome segregation on multiple occasions (Figure 22b). Nucleoid formation also appears to be aberrant in those lacking *fis* (Figure 22b and 22c).

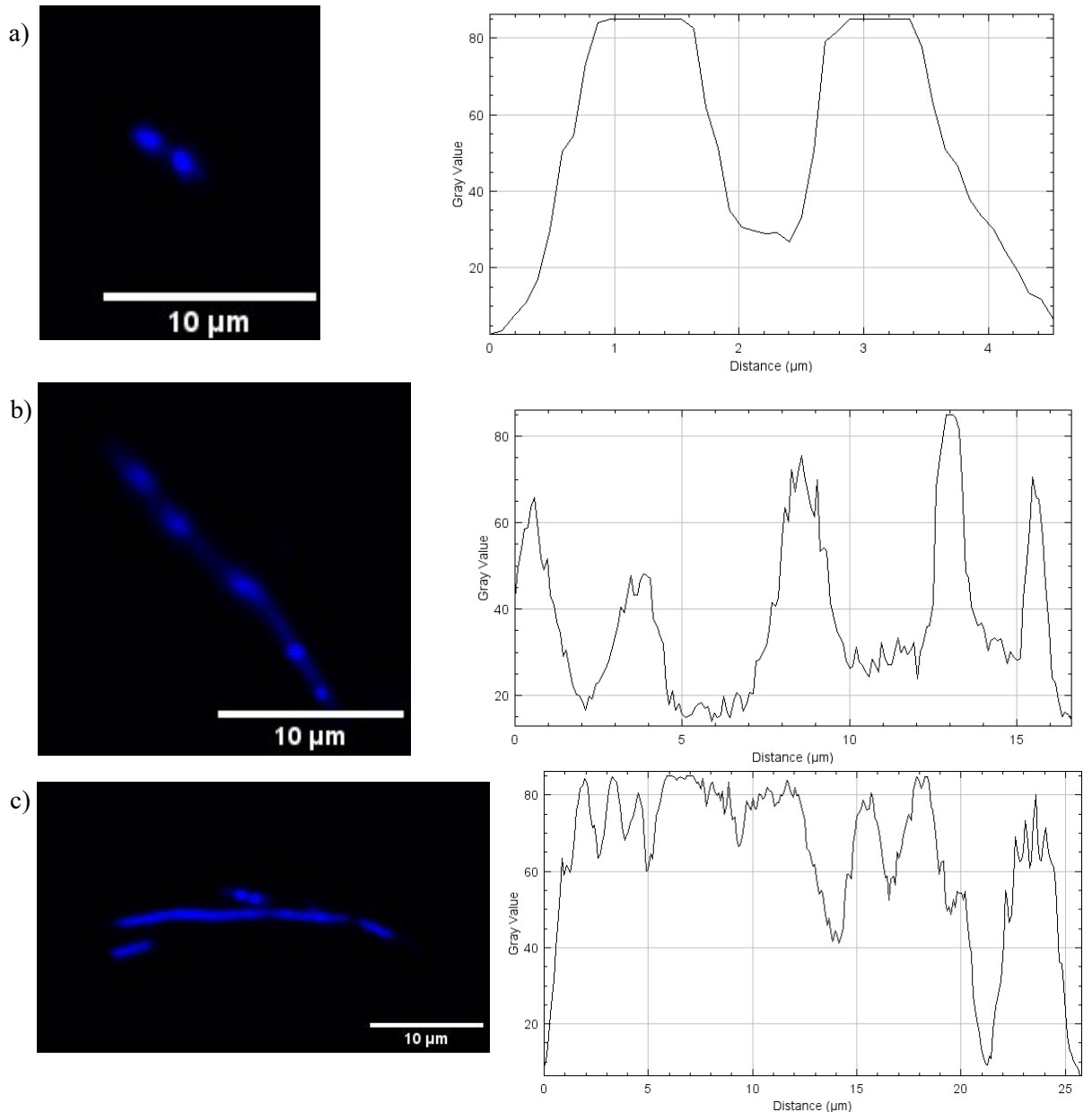


Figure 22: DNA stained with DAPI showing distribution during division a) Uninduced LT2230 b) uninduced LT2260 c) uninduced LT2259. Grey values were measured along the long axis of the cells. Scale bar 10 μm.

In LT447 (MG1655: λ cI857 *ind1 ninH⁺ fis⁺*) before prophage induction, most dividing cells resembled those from LT2230 (MG1655: λ cI857 *ind1 Δ ninH fis⁺*), however a few of the outliers in cell length displayed aberrant nucleoid segregation (Figure 23a). After induction of the λ prophage there were some outliers in cell length that also showed aberrant nucleoid separation (Figure 23b). In contrast to the uninduced cells, the peaks formed after phage induction are messier indicating that the

nucleoids have not condensed properly. This difference could be due to the presence of NinH in LT447, however this is inconclusive as most *E. coli* cells did not show this change after induction of the λ prophage.

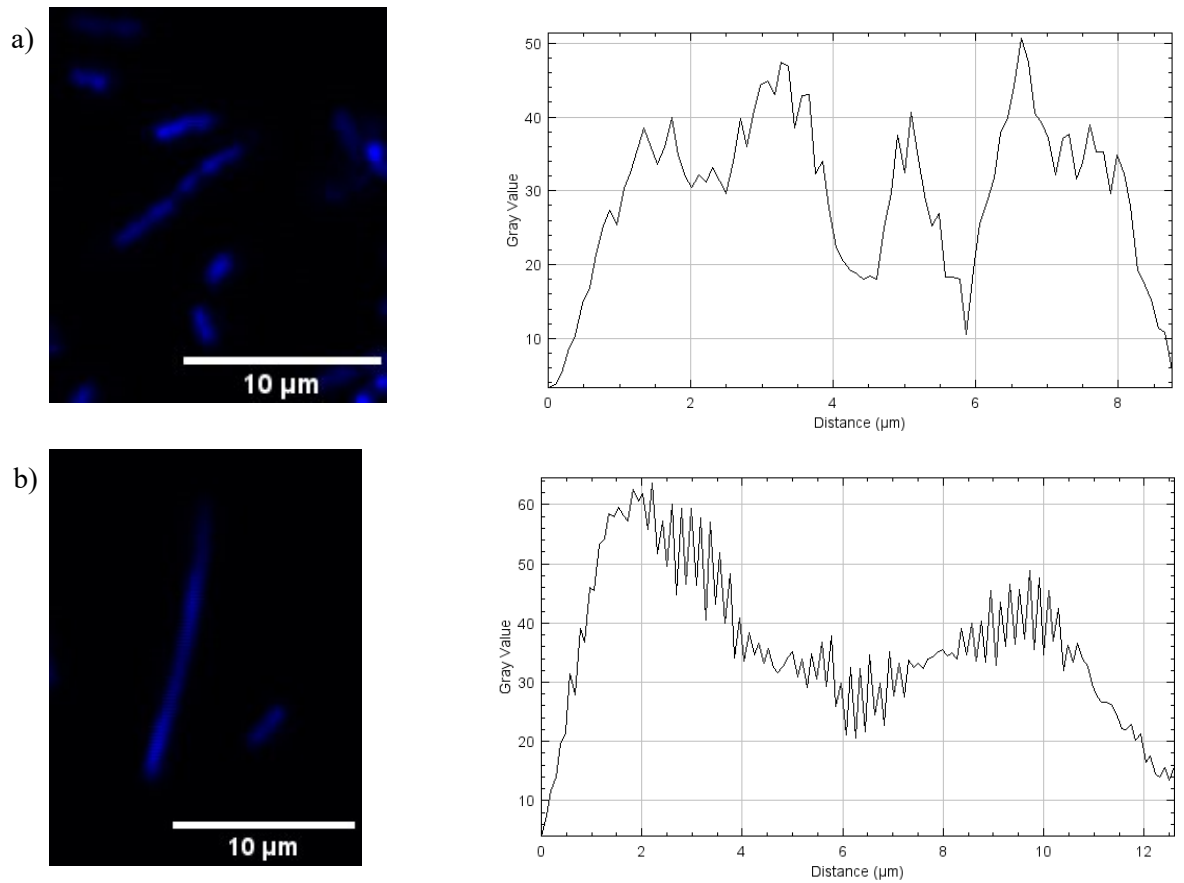


Figure 23: DNA stained with DAPI showing distribution of DNA during division. a) uninduced LT447 b) induced LT447. Grey values were measured along the long axis of the cells. Scale bar 10 μm.

4. Discussion

Despite the ongoing rise in AMR, international efforts to combat the serious problem are failing to meet the recommended scale of actions prescribed by the WHO. Research into novel antibacterials is a crucial component in tackling this crisis. Discussed below is an analysis of each of the Kil proteins investigated in this study with regards to their toxicity, predicted structure and potential mechanism of action. The detrimental effects of NinH on *E. coli* cell morphology are also discussed with a view to utilising this phage protein as an antibacterial.

4.1 λ Kil

λ Kil is the best studied of the Kil proteins to date. *E. coli* containing a defective λ prophage, under control of a temperature-sensitive phage CI repressor, was found to elongate after the repressor was inactivated resulting in a loss of viability (Haeusser et al., 2014). Screening of a pBR322 library of *E. coli* chromosomal fragments for suppression of toxicity revealed that FtsZ overexpression could promote tolerance. In addition, expression of SdiA, which increases *ftsQAZ* operon transcription (Wang, de Boer and Rothfield, 1991), also suppressed toxicity. Neither FtsQ nor FtsA could suppress λ Kil-mediated toxicity, suggesting that FtsZ was its primary target. Haeusser et al. (2014) went on to use immunofluorescent microscopy to image FtsZ and inhibition of Z-ring formation after Kil induction. Furthermore, they found that λ Kil does not alter levels of FtsZ or act through the known endogenous systems of FtsZ inhibition involving Min or SulA. Instead, wild-type λ Kil activity *in vivo* was dependent on the presence of ZipA, and that λ Kil was capable of binding both FtsZ and ZipA.

E. coli containing mutant alleles of *ftsZ* were examined to see if they could confer resistance to λ Kil toxicity. Two mutations were successful in preventing cell filamentation, *ftsZ_{V208A}* and *ftsZ_{L169R}*. These mutations occur in the T7-loop region (*ftsZ_{V208A}*) and the N-terminal domain (*ftsZ_{L169R}*) (Haeusser et al., 2014).

Subsequent studies found that λ Kil disrupts FtsZ protofilaments, which are typically ~60 FtsZ subunits long (Ahijado-Guzmán et al., 2013), producing instead shorter oligomers with reduced GTPase activity (Hernández-Rocamora et al., 2015). This disruption could be detected at relatively low concentrations of λ Kil and exacerbated by increased protein concentrations. Hernández-Rocamora et al (2015) also found that λ Kil had a greater affinity for FtsZ-GDP monomers than FtsZ-GTP monomers. Under these buffer conditions, GTPase activity decreased upon addition of λ Kil, in contrast to previous analyses (Haeusser et al., 2014) where GTPase activity increased after addition of λ Kil. This was attributed to differences in methodology. No GTPase activity was detected from λ Kil itself. It was therefore proposed that λ Kil acts by a sequestering mechanism similar to Sula which also reduces FtsZ GTPase activity (Hernández-Rocamora et al., 2015).

MciZ, a *B. subtilis* cell division inhibitor, at low concentrations has been reported to use a capping mechanism to inhibit FtsZ polymerisation and is theorised to sequester FtsZ at higher concentrations (Bisson-Filho et al., 2015). Other cytoskeletal modulatory proteins have been found to have similar sequestering and capping effects (Fischer et al., 2006). It is feasible that λ Kil acts in similar fashion, utilising a capping mechanism to disrupt FtsZ protofilament formation at low concentrations while at high concentrations sequestering the available FtsZ.

From the viability assays, λ Kil toxicity was confirmed. Unfortunately, due to issues with FtsZ purity or excess polymer formation, binding of λ Kil to FtsZ was unable to be confirmed by gel filtration. The AlphaFold models were also inconclusive with respect to interactions with an FtsZ monomer, which may be affected by some uncertainty over the λ Kil structural model. However, λ Kil is likely to bind to the N-terminal domain of FtsZ that contains the L169 residue implicated in binding. Hernández-Rocamora et al. 2015, through the use of analytical ultracentrifugation, concluded that λ Kil has a tendency to self-associate when purified however no evidence of this was found in the SDS-PAGE analyses. Although this could explain the lack of binding in the AlphaFold models as only a λ Kil monomer was modelled with FtsZ.

4.2 Mu Kil

In 1976 defective Mu prophages were isolated and it was described that bacterial cell death was still induced when these lysogens were incubated at 43°C (Westmaas, van der Maas, and van de Putte, 1976). The gene responsible had to be located upstream of gene *C* since the rest of the prophage was missing in this strain; genes *A* and *B* were also ruled out as mutations in those genes still resulted in cell death. The causative gene was therefore predicted to reside in the early region of the genome (Westmaas, van der Maas, and van de Putte, 1976). The Mu Kil gene was finally precisely mapped in 1989, being located within the first ORF after the *B* gene. Waggoner et al. (1989) found that expression of Mu Kil led to bacterial cells becoming enlarged and spherical. It was thought that Mu Kil could target a component of cell wall biosynthesis during elongation. They also found that even basal levels of Mu Kil could cause the dramatic morphological changes (Waggoner et al., 1989).

Experiments conducted in this study showed Mu Kil to be highly toxic to *E. coli*. Even in uninduced cultures, Mu Kil was toxic, impacting the time it took to grow the culture to the same OD_{600nm} as the other strains. Induction of the Mu *kil* gene reduced *E. coli* viability entirely in all but two repeats. This could have been caused by a mutation within the *E. coli* chromosome conferring partial resistance, loss of the plasmid or potentially a mutation in the Mu *kil* gene that reduced its toxicity or expression. To further identify possible resistance mechanisms, surviving colonies could be isolated from the plate and sequenced. If there was a mutation in either the *E. coli* genome or the Mu *kil* gene these could help in identifying the mechanism by which Mu Kil causes such a dramatic cellular response.

The AlphaFold model of Mu Kil had a >90% confidence level across the bulk of the protein, with its structure seemingly very similar to that found already in the PDB. When Mu Kil and FtsZ were modelled together, the confidence level of Mu Kil reduced to <70% across the protein and <50% where Mu Kil was modelled to bind to FtsZ. This drastic reduction in confidence likely implies that Mu Kil does not bind to FtsZ and suggests its mode of action to induce cell death is different to that of λ Kil. This would be consistent with the studies showing different morphological changes brought about by Mu Kil compared to λ Kil.

4.3 Rac Kil

Prophage Rac Kil has been observed to cause similar morphological changes in *E. coli* as λ Kil, both causing filamentation prior to cell death. Similarly, overexpression of FtsZ was able to recover the cell division defect induced by Rac Kil. In addition, high levels of Rac Kil abolished the *E. coli* rod shape and acted independently of the Min system (Conter, Bouche and Dassain, 1996). More recently, in a paper investigating the effects of bicyclomycin (BCM) on *E. coli* mutants with single gene deletions, it

was found that in the absence of the Rac *kil* gene, the *E. coli* had partial resistance to BCM (Tran et al., 2011). BCM functions by inhibiting the transcription termination factor Rho. Without BCM, Rho terminates transcription upstream of toxic foreign genes (Cardinale et al., 2008), including the *kil* gene from Rac. It was also found that deletion of a negative regulator of FtsZ, *hfq* (Takada, Wachi and Nagai, 1999), caused cells to show greater resistance to BCM. This feature links back to the previous results where overexpression of FtsZ abolished Rac Kil toxicity.

In this study, Rac Kil expression resulted in a considerable log reduction (4.85-fold) in *E. coli* viability. Unlike Mu Kil, Rac Kil did not entirely prevent colony formation but did still reduce colony viability by 100,000-fold. Despite purification of Rac Kil, the issues with FtsZ prevented the identification of potential binding between the two proteins and the low concentrations of each meant the results could not be interpreted by SDS-PAGE. However, AlphaFold models of Rac Kil and FtsZ showed some promise. The predicted structure of Rac Kil showed a confidence level of >90% across the majority of the protein. When modelled with FtsZ this confidence level reduced to 60-80% across Rac Kil, and FtsZ confidence around the potential binding site to 60-80%. This confidence level is encouraging for the potential of Rac Kil to associate with FtsZ. When viewed in PyMOL, this model of Rac Kil appears to bind near L169 in the N-terminal region of FtsZ. An FtsZ mutant with L178E was found to be assembly incompetent (Du et al., 2015), this residue is on the other side of the flexible loop to L169. It is possible that Rac Kil binds in the vicinity of this site, potentially inhibiting FtsZ polymerisation. However, the efficacy of Rac Kil may not be as universal across bacterial species as the FtsZ N-terminal domain is poorly conserved (Bushe and Levin, 2012).

Through analysis from the DALI server, Rac Kil shares a structural similarity to part of an eif-5A family protein from *Naegleria fowleri*. This could potentially clash with hopes of Rac Kil being used as an antibacterial due to proteins in the eif-5A family being found across most eukaryotic species including in humans.

Further size exclusion experiments could be conducted in order to confirm the interaction of Rac Kil with FtsZ; using freshly purified FtsZ to determine whether peaks form in the expected places for FtsZ and Rac Kil plus FtsZ. Alternative techniques could also be employed to evaluate potential protein-protein interactions.

4.4 P22 Kil

P22 is a temperate phage which usually resides within *Salmonella enterica* Serovar Typhimurium (Susskind and Botstein, 1978). Despite infecting different hosts, phage P22 and phage λ have many genes and regulatory sequences that show similar gene organisation and possess analogous functions. Despite this, there is often a lack of sequence homology between many of these functional orthologs (Semerjian, Malloy and Poteete, 1989). When the genetic structure of P22's P_L operon was investigated, a *kil* gene was found located within the P_L operon, mapping to the same place as *kil* within phage λ . P22 Kil expression resulted in cell filamentation and eventual cell death, consistent with the similarities with λ Kil. However, unlike λ Kil, P22 Kil appeared to affect the lytic growth of P22 (Semerjian, Malloy and Poteete, 1989). P22 Kil, expressed from the *kil* gene cloned from P22 lytic phage derivatives induced the SOS response in both *E. coli* and *Salmonella enterica* (Campoy et al., 2006). During the SOS response, accumulated single-stranded DNA is bound by RecA. This promotes the autocatalytic cleavage of LexA (and similarly cI in λ), a transcriptional repressor of the SOS-regulated genes. This allows over 50 genes to be expressed including Sula, a cell division inhibitor (Maslowska, Makiela-Dzbenka and

Fijalkowska, 2019). In the study by Campoy et al. (2006), quantitative RT-PCR analysis showed a clear increase in *recA* expression after induction of the lytic P22 derivative. This was confirmed to be in response to the expression of *kil* after testing P22 with a mutation in the *kil* gene. This suggests that the cell filamentation effect of P22 is caused by activation of SulA and its action in blocking cell division.

In this study P22 Kil showed little toxicity, with no decrease in colony numbers in viability assays. However, there was a decrease in colony size, suggesting that P22 *kil* expression does affect *E. coli* growth. This difference in activity to previous studies could be due to the dual function of P22 Kil as a promotor of lytic growth and its effects on cell filamentation.

The AlphaFold model of P22 showed a >90% degree of confidence in the 3-D structure. When modelling with FtsZ, confidence in the 3D-structure of P22 fell to <60% with those parts near the potential binding site <50%. This could point towards P22 Kil not binding FtsZ and supports the theory that cell filamentation caused by P22 Kil is brought about through SulA.

4.5 DicB

Prophage Qin DicB is known to inhibit septation, resulting in long filamentous cells (De Boer, Crossley and Rothfield, 1990). The involvement of MinC was instrumental in the septum inhibition process involving DicB (De Boer, Crossley and Rothfield, 1990). Microscopy experiments indicated that DicB competes with MinD for binding to MinC. It was also found that DicB directly interacts with the MinC C-terminal domain and that the MinC-DicB complex has a high affinity for septal ring structures *in vivo* (Johnson, Lackner and De Boer, 2002). ZipA was crucial for the recruitment of the MinC-DicB complex to FtsZ rings and led to a simple model for FtsZ-ring

inhibition by DicB. DicB associates with MinC, this complex has a specific affinity for ZipA. ZipA then interacts with membrane-associated FtsZ polymers. This brings MinC close enough to start FtsZ depolymerisation (Johnson et al., 2004). *In vitro* studies found that the N-terminal domain of DicB is essential for DicB function (Yang et al., 2016). Further microscopy experiments involving λ Kil, Rac Kil and DicB revealed that induction of DicB in *E. coli* cells resulted in cells of $>50 \mu\text{m}$ in length, considerably longer than both λ Kil and Rac Kil (Black, 2023).

In this study, DicB was found to be extremely toxic to *E. coli*, with a decrease in viability similar to that seen with Mu Kil and Rac Kil. Unlike Rac Kil, DicB reduced viability in the absence of induction, implying that even low levels of this protein are toxic.

The AlphaFold model of DicB displayed structural similarities to λ Kil, with both proteins consisting of two α -helices. The structural confidence for DicB was $>90\%$ over the majority of the protein. When modelled with FtsZ, confidence for DicB decreased to $<50\%$ across the whole protein, indicating that it is unlikely that DicB binds to FtsZ directly. This agrees with findings from pull-down assays where no direct interaction between DicB and FtsZ was recorded (Yang et al., 2016). However, in this study DicB inhibitory activity was reduced by the fusion of a maltose binding protein to the N-terminus of DicB.

4.6 YdfD

YdfD was only recently discovered in the Qin prophage. The *ydfD* gene was found to be located directly downstream of *dicB*, overlapping *dicB* by 4bp. This indicated that both genes are under the control of DicA, a transcriptional repressor. YdfD was shown to be toxic by inducing cell lysis, killing 99.9% of bacteria within 2 hours. Examined

under a microscope these cells appeared to have ruptured, with incisions at the middle or posterior of the cells where leakage of genomic DNA occurred (Masuda, Awano and Inouye, 2016). Other microscopy experiments using live/dead staining (Black, 2023), found that YdfD did not alter *E. coli* cell morphology. However, YdfD did cause decreased viability, with a higher percentage of cells with apparent loss of integrity. With no change in morphology, it is likely that YdfD does not act upon FtsZ.

The YdfD structure was thought to contain a hydrophobic N-terminal domain and a suggested cytoplasmic C-terminal domain. The N-terminus was thought necessary for localisation to the inner leaflet of the cytoplasmic membrane and the C-terminus required for toxicity. Secretion of the C-terminal domain into the periplasmic space did not cause cell lysis, indicating its target is within the cytoplasm (Masuda, Awano and Inouye, 2016).

When YdfD was co-expressed with DicB, no cell lysis was observed. Instead, the cells were elongated, suggesting DicB could still halt cell division. This could indicate that for YdfD to cause lysis cell division must continue normally, which fits with the negative effects of YdfD being abolished after addition of SulA (Masuda, Awano and Inouye, 2016). Recently YdfD was found to specifically inhibit the IspG-catalysed step in the MEP pathway of *E. coli* (Lu et al., 2022). The MEP pathway is how most bacteria synthesise dimethylallyl pyrophosphate (DMAPP) and its isomer isopentenyl pyrophosphate (IPP; Rohmer, 2008). Both are crucial in the synthesis of terpenoid compounds which themselves are required for maintaining cell membrane stability and peptidoglycan synthesis (Anderson, Hussey and Baddiley, 1972). The pathway utilises seven enzymes in a linear fashion, with the sixth being IspG. This enzyme, assisted by an Fe-S cluster, converts 4-diphosphocytidyl-methylerythritol 2-phosphate (ME-cPP) into methylerythritol 2,4-cyclodiphosphate (HMBPP; Masini and Hirsch,

2014). The direct interaction between YdfD and IspG was studied using pull-down assays, size exclusion chromatography, isothermal titration calorimetry and FRET. YdfD was found to bind IspG both *in vivo* and *in vitro*. Addition of HMBPP or the overexpression of *ispG* both circumvented the lysis induced by YdfD. It was therefore suggested that YdfD directly targets IspG, halting production of HMBPP and consequently inhibiting cell wall synthesis (Lu et al., 2022).

In this study, there was no significant change in viability when YdfD was induced. This contrasts with results obtained previously (Masuda, Awano and Inouye, 2016; Black, 2023), where lysis was confirmed on solid media. This difference could be due to the different expression systems used in each study.

AlphaFold models of YdfD had a high confidence (>90%) across the majority of the 3-D structure. When modelled with FtsZ, YdfD confidence fell to <50% across most of the structure, indicating that YdfD does not interact with FtsZ. This would agree with published studies in suggesting YdfD lysis is induced *via* IspG binding and halting cell wall synthesis.

Overall, YdfD could represent a novel natural antibacterial. Its toxicity to *E. coli* is high and with the MEP pathway being absent in humans, YdfD's toxicity to humans should be minimal.

4.7 T7 Gp0.4

Phage T7 was found to contain a gene whose product has a similar function to λ Kil. It was termed gene product 0.4 (Gp0.4). This gene was first described in 1972 (Studier, 1972) but had no known function. Decades later its function was investigated. Tandem-affinity purification (TAP) assays were used to identify cellular interactions with Gp0.4. After pull-down assays to remove any false-positives from the TAP

assays, FtsZ was the only protein bound by Gp0.4. Gp0.4 toxicity was assessed, and a drop of six orders of magnitude in bacterial viability was noted. Interactions of purified Gp0.4 and purified FtsZ were studied *in vitro* using a fluorescence-based assay to measure FtsZ assembly. Increasing concentrations of Gp0.4 increasingly inhibit assembly of FtsZ polymers. In addition, light microscopy of *E. coli* after *gp0.4* expression revealed elongated and filamented cells (Kiro et al., 2013).

Gp0.4 and its binding to FtsZ has been previously modelled using an *ab initio* approach. This indicated that Gp0.4 adopts a ‘U’ shaped conformation which can insert itself into a cleft between helices on FtsZ (Simpkin and Rigden, 2016). The AlphaFold model in this study was also ‘U’ shaped, and reminiscent of both λ Kil and DicB structures. Modelling the interaction with FtsZ, the position of Gp0.4 is entirely

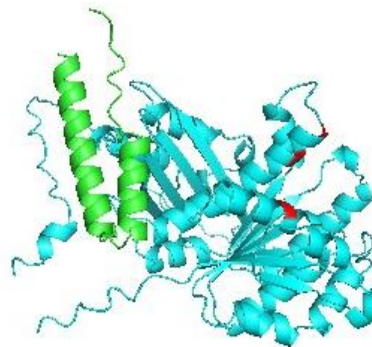


Figure 24: FtsZ (cyan) and Gp0.4 (green) protein-protein interaction model. FtsZ residues N24, L178 and F182 (red).

different to that described by Simpkin and Rigden (2016; Figure 24). This could be due to differences in the modelled structures and predicted assemblies of both Gp0.4 and FtsZ. However, here, the modelling of Gp0.4 and FtsZ showed that Gp0.4 could potentially interact with FtsZ near V208, a region within the T7 loop. Thus, it is possible that Gp0.4 can inhibit FtsZ polymerisation by binding where another FtsZ subunit would assemble or by binding and blocking the GTP active site.

4.8 NinH and *E. coli* cell elongation

In this thesis, average *E. coli* cell length was slightly above normal with an average of between 2-3 μm , the usual being 1-2 μm (Shiomi, Mori and Niki, 2009). This could be caused by cells being grown in good conditions or the inclusion of the prophage itself causing this slight increase in length. Most likely however, as cell length was measured manually in ImageJ, dividing cells could have been mistaken as one cell skewing the average. This was more likely to be present in the LT447 (MG1655: λ cI857 *ind1 ninH⁺ fis⁺*) and LT2230 (MG1655: λ cI857 *ind1 Δ ninH fis⁺*) as from the overall images cell division was seeming to occur more regularly in these two samples.

After induction of phage λ , an increase in the length of LT447 (*Δ ninH fis⁺*) cells was seen in comparison to that of LT2230 (*ninH⁺ fis⁺*). Two outliers were found completely outside the range of the uninduced LT447 *E. coli*. This could indicate that NinH causes *E. coli* cells to elongate, however, the increase is not significant enough to prove this.

No significant difference could be found between cells lacking in Fis in both induced and uninduced cultures, whether or not prophage λ was carrying *ninH*. These elongated cells are common for strains lacking *fis* (Filutowicz et al., 1992).

DNA distribution in LT447 cells, based on DAPI staining, was uneven, suggesting that the potential cause of cell elongation could be due to NinH being able to bind and bend DNA but differently to Fis causing aberrant nucleoid formation. If DNA was present at the mid-cell during division, SlmA from the NO system could prevent division occurring, resulting in elongated *E. coli* (Silber et al., 2020).

These findings correlate with the toxicity results from Chakraborti et al (2020). The change in DNA distribution could be a result of NinH's predicted ability to bind and bend DNA, causing aberrant nucleoid formation. More extreme versions of this

aberrant nucleoid formation are seen in cells lacking Fis. Induction of NinH in Fis lacking strain (LT2260) does not appear to replace missing Fis, again this could be due to the differences in Fis and NinH binding abilities.

5. Conclusions & future work

This study aimed to investigate the toxicity, structure and function of several small phage polypeptides. Out of the seven proteins investigated, three were found to be incredibly toxic to *E. coli*. Mu Kil appeared to be the most toxic, causing cell death even when expression was not induced. No concrete conclusions could be drawn about the role of NinH after prophage induction. Although the average cell length after induction was longer for those cells with *fis* and *ninH*. In addition, some of the *E. coli* cells containing *fis* and *ninH* after induction of λ showed aberrant nucleoid formation. However, not to the same extent that the absence of *fis* causes in bacterial cells.

Structural investigation using the DALI server revealed that most of these proteins do not share any structural similarity with each other, nor do they have a significant structural similarity to any other known proteins within the PDB. Rac Kil is the exception with similarity to a part of a eukaryotic protein which could cause Rac Kil to interfere with other processes in the human body and therefore be toxic.

Future directions for identifying the mode of action of the Kil proteins could include the isolation of bacteria showing resistance to the toxic effects and whole genome sequencing to identify any genes responsible. Studying mutations that affect interacting sites in the Kil proteins is another alternative approach. Furthermore, to characterise Kil protein interactions with FtsZ, size exclusion chromatography experiments should be performed again with freshly purified FtsZ, or through other alternative binding experiments. Given the insolubility of these Kil proteins, determination of their structure alone or combined with FtsZ may prove challenging to probe with X-ray crystallography. However, solving these structures would prove

insightful in defining the mechanism of bacterial killing and how these might be harnessed as novel antibacterial peptides.

Going forward, to use these proteins as antibacterials, we would be aiming to use shorter versions of these peptides that could mimic blockage of cell division apparatus. These shorter peptides could then be taken up by cells. Alternatively, some membrane damage could be imposed to promote peptide uptake.

6. References

- Ahijado-Guzmán, R., Alfonso, C., Reija, B., Salvarelli, E., Mingorance, J., Zorrilla, S., Monterroso, B. and Rivas, G., 2013. Control by potassium of the size distribution of *Escherichia coli* FtsZ polymers is independent of GTPase activity. *Journal of Biological Chemistry*, 288(38), pp.27358-27365.
- Amemiya, H.M., Schroeder, J. and Freddolino, P.L., 2021. Nucleoid-associated proteins shape chromatin structure and transcriptional regulation across the bacterial kingdom. *Transcription*, 12(4), pp.182-218.
- Anderson, R.G., Hussey, H. and Baddiley, J., 1972. The mechanism of wall synthesis in bacteria. The organization of enzymes and isoprenoid phosphates in the membrane. *Biochemical Journal*, 127(1), pp.11-25.
- Bi, E. and Lutkenhaus, J., 1991. FtsZ ring structure associated with division in *Escherichia coli*. *Nature*, 354(6349), pp.161-164.
- Bi, E. and Lutkenhaus, J., 1993. Cell division inhibitors SulA and MinCD prevent formation of the FtsZ ring. *Journal of bacteriology*, 175(4), pp.1118-1125.
- Bisson-Filho, A.W., Discola, K.F., Castellen, P., Blasios, V., Martins, A., Sforça, M.L., Garcia, W., Zeri, A.C.M., Erickson, H.P., Dessen, A. and Gueiros-Filho, F.J., 2015. FtsZ filament capping by MciZ, a developmental regulator of bacterial division. *Proceedings of the National Academy of Sciences*, 112(17), pp.E2130-E2138.
- Bisson-Filho, A.W., Hsu, Y.P., Squyres, G.R., Kuru, E., Wu, F., Jukes, C., Sun, Y., Dekker, C., Holden, S., VanNieuwenhze, M.S. and Brun, Y.V., 2017. Treadmilling by FtsZ filaments drives peptidoglycan synthesis and bacterial cell division. *Science*, 355(6326), pp.739-743.
- Black, D. J., 2023. Characterisation of the bacteriostatic and bactericidal mode of action of antibacterial proteins and compounds using Laser Scanning Confocal Microscopy. Durham theses, Durham University. Available at Durham E-Theses Online: <http://etheses.dur.ac.uk/15388/> (Accessed: 21 May 2024)
- Blattner, F.R., Plunkett III, G., Bloch, C.A., Perna, N.T., Burland, V., Riley, M., Collado-Vides, J., Glasner, J.D., Rode, C.K., Mayhew, G.F. and Gregor, J., 1997. The complete genome sequence of *Escherichia coli* K-12. *Science*, 277(5331), pp.1453-1462.
- Borrmann, S., Lundgren, I., Oyakhirome, S., Impouma, B., Matsiegui, P.B., Adegnika, A.A., Issifou, S., Kun, J.F., Hutchinson, D., Wiesner, J. and Jomaa, H., 2006. Fosmidomycin plus clindamycin for treatment of pediatric patients aged 1 to 14 years with *Plasmodium falciparum* malaria. *Antimicrobial agents and chemotherapy*, 50(8), pp.2713-2718.

- Brady, A., Felipe-Ruiz, A., Gallego del Sol, F., Marina, A., Quiles-Puchalt, N. and Penadés, J.R., 2021. Molecular basis of lysis–lysogeny decisions in Gram-positive phages. *Annual review of microbiology*, 75, pp.563-581.
- Browning, D.F., Grainger, D.C. and Busby, S.J., 2010. Effects of nucleoid-associated proteins on bacterial chromosome structure and gene expression. *Current opinion in microbiology*, 13(6), pp.773-780.
- Brüssow, H., 2005. Phage therapy: the *Escherichia coli* experience. *Microbiology*, 151(7), pp.2133-2140.
- Buske, P.J. and Levin, P.A., 2012. Extreme C terminus of bacterial cytoskeletal protein FtsZ plays fundamental role in assembly independent of modulatory proteins. *Journal of Biological Chemistry*, 287(14), pp.10945-10957.
- Cameron, T.A. and Margolin, W., 2024. Insights into the assembly and regulation of the bacterial divisome. *Nature Reviews Microbiology*, 22(1), pp.33-45.
- Campoy, S., Hervàs, A., Busquets, N., Erill, I., Teixidó, L. and Barbé, J., 2006. Induction of the SOS response by bacteriophage lytic development in *Salmonella enterica*. *Virology*, 351(2), pp.360-367.
- Cardinale, C.J., Washburn, R.S., Tadigotla, V.R., Brown, L.M., Gottesman, M.E. and Nudler, E., 2008. Termination factor Rho and its cofactors NusA and NusG silence foreign DNA in *E. coli*. *Science*, 320(5878), pp.935-938.
- Casjens, S.R. and Hendrix, R.W., 2015. Bacteriophage lambda: Early pioneer and still relevant. *Virology*, 479, pp.310-330.
- Catalao, M.J., Gil, F., Moniz-Pereira, J., Sao-Jose, C. and Pimentel, M., 2013. Diversity in bacterial lysis systems: bacteriophages show the way. *FEMS microbiology reviews*, 37(4), pp.554-571.
- Chakraborti, S., Balakrishnan, D., Trotter, A.J., Gittens, W.H., Yang, A.W., Jolma, A., Paterson, J.R., Świątek, S., Plewka, J., Curtis, F.A., Bowers, L.Y., Palsson, L., Hughes, T.R., Taube, M., Kozak, M., Heddle, J.G. and Sharples, G.J., 2020. A bacteriophage mimic of the bacterial nucleoid-associated protein Fis. *Biochemical Journal*, 477(7), pp.1345-1362.
- Chen, Y., Milam, S.L. and Erickson, H.P., 2012. SulA inhibits assembly of FtsZ by a simple sequestration mechanism. *Biochemistry*, 51(14), pp.3100-3109.
- Chibani-Chennoufi, S., Bruttin, A., Dillmann, M.L. and Brüssow, H., 2004. Phage-host interaction: an ecological perspective. *Journal of bacteriology*, 186(12), pp.3677-3686
- Cho, B.K., Knight, E.M., Barrett, C.L. and Palsson, B.Ø., 2008. Genome-wide analysis of Fis binding in *Escherichia coli* indicates a causative role for A-/AT-tracts. *Genome research*, 18(6), pp.900-910.
- Christopher, K.C., Rita, W.Y., Leung, S.S., Mamie, H.U.I. and Ip, M., 2021. Overcoming the rising incidence and evolving mechanisms of antibiotic resistance

by novel drug delivery approaches—an overview. *Advanced Drug Delivery Reviews*, p.114078.

Conter A, Bouche J-P, Dassain M (1996). Identification of a new inhibitor of essential division gene *ftsZ* as the *kil* gene of defective prophage Rac. *Journal of Bacteriology* 178: 5100–5104.

Dajkovic, A., Lan, G., Sun, S.X., Wirtz, D. and Lutkenhaus, J., 2008. MinC spatially controls bacterial cytokinesis by antagonizing the scaffolding function of FtsZ. *Current Biology*, 18(4), pp.235-244.

De Boer, P.A., Crossley, R.E. and Rothfield, L.I., 1989. A division inhibitor and a topological specificity factor coded for by the minicell locus determine proper placement of the division septum in *E. coli*. *Cell*, 56(4), pp.641-649.

De Boer, P.A., Crossley, R.E. and Rothfield, L.I., 1990. Central role for the *Escherichia coli minC* gene product in two different cell division-inhibition systems. *Proceedings of the National Academy of Sciences*, 87(3), pp.1129-1133.

Du, S., Park, K.T. and Lutkenhaus, J., 2015. Oligomerization of FtsZ converts the FtsZ tail motif (conserved carboxy-terminal peptide) into a multivalent ligand with high avidity for partners ZipA and SlmA. *Molecular microbiology*, 95(2), pp.173-188.

Echols, H., 1972. Developmental pathways for the temperate phage: lysis vs lysogeny. *Annual review of genetics*, 6(1), pp.157-190.

Egan, A.J. and Vollmer, W., 2013. The physiology of bacterial cell division. *Annals of the New York Academy of Sciences*, 1277(1), pp.8-28.

Erickson, H.P., Anderson, D.E. and Osawa, M., 2010. FtsZ in bacterial cytokinesis: cytoskeleton and force generator all in one. *Microbiology and molecular biology reviews*, 74(4), pp.504-528.

Faubladier, M. and Bouché, J.P., 1994. Division inhibition gene *dicF* of *Escherichia coli* reveals a widespread group of prophage sequences in bacterial genomes. *Journal of bacteriology*, 176(4), pp.1150-1156.

Filutowicz, M., Ross, W., Wild, J. and Gourse, R.L., 1992. Involvement of Fis protein in replication of the *Escherichia coli* chromosome. *Journal of bacteriology*, 174(2), pp.398-407.

Fischer, R.S., Yarmola, E.G., Weber, K.L., Speicher, K.D., Speicher, D.W., Bubb, M.R. and Fowler, V.M., 2006. Tropomodulin 3 binds to actin monomers. *Journal of Biological Chemistry*, 281(47), pp.36454-36465.

Fleming, A., 1929. On the antibacterial action of cultures of a penicillium, with special reference to their use in the isolation of *B. influenzae*. *British journal of experimental pathology*, 10(3), p.226.

Fong, I.W., 2023. Antimicrobial resistance: a crisis in the making. *New Antimicrobials: For the Present and the Future*, pp.1-21.

Fu, X., Shih, Y.L., Zhang, Y. and Rothfield, L.I., 2001. The MinE ring required for proper placement of the division site is a mobile structure that changes its cellular

- location during the *Escherichia coli* division cycle. *Proceedings of the National Academy of Sciences*, 98(3), pp.980-985.
- Fujita, J., Maeda, Y., Mizohata, E., Inoue, T., Kaul, M., Parhi, A.K., LaVoie, E.J., Pilch, D.S. and Matsumura, H., 2017. Structural flexibility of an inhibitor overcomes drug resistance mutations in *Staphylococcus aureus* FtsZ. *ACS chemical biology*, 12(7), pp.1947-1955.
- Gelpi, A., Gilbertson, A. and Tucker, J.D., 2015. Magic bullet: Paul Ehrlich, Salvarsan and the birth of venereology. *Sexually transmitted infections*, 91(1), pp.68-69.
- Greer, H., 1975. The *kil* gene of bacteriophage lambda. *Virology*, 66(2), pp.589-604.
- Haas, L.F., 1999. Papyrus of Ebers and Smith. *Journal of Neurology, Neurosurgery & Psychiatry*, 67(5), pp.578-578.
- Haeusser, D.P., Hoashi, M., Weaver, A., Brown, N., Pan, J., Sawitzke, J.A., Thomason, L.C., Court, D.L. and Margolin, W., 2014. The Kil peptide of bacteriophage λ blocks *Escherichia coli* cytokinesis via ZipA-dependent inhibition of FtsZ assembly. *PLoS genetics*, 10(3), p.e1004217.
- Han, H., Wang, Z., Li, T., Teng, D., Mao, R., Hao, Y., Yang, N., Wang, X. and Wang, J., 2021. Recent progress of bacterial FtsZ inhibitors with a focus on peptides. *The FEBS Journal*, 288(4), pp.1091-1106.
- Hernández-Rocamora, V.M., Alfonso, C., Margolin, W., Zorrilla, S. and Rivas, G., 2015. Evidence that bacteriophage λ Kil peptide inhibits bacterial cell division by disrupting FtsZ protofilaments and sequestering protein subunits. *Journal of Biological Chemistry*, 290(33), pp.20325-20335.
- Holm, L., Laiho, A., Törönen, P. and Salgado, M., 2023. DALI shines a light on remote homologs: One hundred discoveries. *Protein Science*, 32(1), p.e4519.
- Huang, K.H., Durand-Heredia, J. and Janakiraman, A., 2013. FtsZ ring stability: of bundles, tubules, crosslinks, and curves. *Journal of bacteriology*, 195(9), pp.1859-1868.
- Hutchings, M.I., Truman, A.W. and Wilkinson, B., 2019. Antibiotics: past, present and future. *Current opinion in microbiology*, 51, pp.72-80.
- Johnson, J.E., Lackner, L.L. and De Boer, P.A., 2002. Targeting of ^DMinC/MinD and ^DMinC/DicB complexes to septal rings in *Escherichia coli* suggests a multistep mechanism for MinC-mediated destruction of nascent FtsZ rings. *Journal of bacteriology*, 184(11), pp.2951-2962.
- Johnson, J.E., Lackner, L.L., Hale, C.A. and De Boer, P.A., 2004. ZipA is required for targeting of ^DMinC/DicB, but not ^DMinC/MinD, complexes to septal ring assemblies in *Escherichia coli*. *Journal of bacteriology*, 186(8), pp.2418-2429.
- Jumper, J., Evans, R., Pritzel, A., Green, T., Figurnov, M., Ronneberger, O., Tunyasuvunakool, K., Bates, R., Žídek, A., Potapenko, A. and Bridgland, A., 2021.

Highly accurate protein structure prediction with AlphaFold. *Nature*, 596(7873), pp.583-589.

Katz, L. and Baltz, R.H., 2016. Natural product discovery: past, present, and future. *Journal of Industrial Microbiology and Biotechnology*, 43(2-3), pp.155-176.

Kaul, M., Mark, L., Parhi, A.K., LaVoie, E.J. and Pilch, D.S., 2016. Combining the FtsZ-targeting prodrug TXA709 and the cephalosporin cefdinir confers synergy and reduces the frequency of resistance in methicillin-resistant *Staphylococcus aureus*. *Antimicrobial agents and chemotherapy*, 60(7), pp.4290-4296.

Kaul, M., Mark, L., Zhang, Y., Parhi, A.K., Lyu, Y.L., Pawlak, J., Saravolatz, S., Saravolatz, L.D., Weinstein, M.P., LaVoie, E.J. and Pilch, D.S., 2015. TXA709, an FtsZ-targeting benzamide prodrug with improved pharmacokinetics and enhanced in vivo efficacy against methicillin-resistant *Staphylococcus aureus*. *Antimicrobial agents and chemotherapy*, 59(8), pp.4845-4855.

Kiro, R., Molshanski-Mor, S., Yosef, I., Milam, S.L., Erickson, H.P. and Qimron, U., 2013. Gene product 0.4 increases bacteriophage T7 competitiveness by inhibiting host cell division. *Proceedings of the National Academy of Sciences*, 110(48), pp.19549-19554.

Kusuma, K.D., Payne, M., Ung, A.T., Bottomley, A.L. and Harry, E.J., 2019. FtsZ as an antibacterial target: status and guidelines for progressing this avenue. *ACS infectious diseases*, 5(8), pp.1279-1294.

Lederberg, E.M. and Lederberg, J., 1953. Genetic studies of lysogenicity in *Escherichia coli*. *Genetics*, 38(1), p.51.

Liu, X., Jiang, H., Gu, Z. and Roberts, J.W., 2013. High-resolution view of bacteriophage lambda gene expression by ribosome profiling. *Proceedings of the National Academy of Sciences*, 110(29), pp.11928-11933.

Lock, R.L. and Harry, E.J., 2008. Cell-division inhibitors: new insights for future antibiotics. *Nature Reviews Drug Discovery*, 7(4), pp.324-338.

Lu, Z., Wang, B., Qiu, Z., Zhang, R., Zheng, J. and Jia, Z., 2022. YdfD, a Lysis Protein of the Qin Prophage, Is a Specific Inhibitor of the IspG-Catalyzed Step in the MEP Pathway of *Escherichia coli*. *International Journal of Molecular Sciences*, 23(3), p.1560.

Lutkenhaus, J., 2007. Assembly dynamics of the bacterial MinCDE system and spatial regulation of the Z ring. *Annu. Rev. Biochem.*, 76, pp.539-562.

Mariani, V., Biasini, M., Barbato, A. and Schwede, T., 2013. IDDT: a local superposition-free score for comparing protein structures and models using distance difference tests. *Bioinformatics*, 29(21), pp.2722-2728.

Masini, T. and Hirsch, A.K., 2014. Development of inhibitors of the 2 C-methyl-D-erythritol 4-phosphate (MEP) pathway enzymes as potential anti-infective agents. *Journal of medicinal chemistry*, 57(23), pp.9740-9763.

- Masłowska, K.H., Makiela-Dzbenka, K. and Fijałkowska, I.J., 2019. The SOS system: a complex and tightly regulated response to DNA damage. *Environmental and molecular mutagenesis*, 60(4), pp.368-384.
- Masuda, H., Awano, N. and Inouye, M., 2016. ydfD encodes a novel lytic protein in *Escherichia coli*. *FEMS Microbiology Letters*, 363(6), p.fnw039.
- McNair, K., Bailey, B.A. and Edwards, R.A., 2012. PHACTS, a computational approach to classifying the lifestyle of phages. *Bioinformatics*, 28(5), pp.614-618.
- Mdarhri, H.A., Benmessaoud, R., Yacoubi, H., Seffar, L., Assimi, H.G., Hamam, M., Boussettine, R., Filali-Ansari, N., Lahlou, F.A., Diawara, I. and Ennaji, M.M., 2022. Alternatives therapeutic approaches to conventional antibiotics: Advantages, limitations and potential application in medicine. *Antibiotics*, 11(12), p.1826.
- Menouni, R., Hutinet, G., Petit, M.A. and Ansaldi, M., 2015. Bacterial genome remodeling through bacteriophage recombination. *FEMS microbiology letters*, 362(1), pp.1-10.
- Michael, C.A., Dominey-Howes, D. and Labbate, M., 2014. The antimicrobial resistance crisis: causes, consequences, and management. *Frontiers in public health*, 2, p.145.
- Migocki, M.D., Freeman, M.K., Wake, R.G. and Harry, E.J., 2002. The Min system is not required for precise placement of the midcell Z ring in *Bacillus subtilis*. *EMBO reports*, 3(12), pp.1163-1167.
- Mirdita, M., Schütze, K., Moriwaki, Y., Heo, L., Ovchinnikov, S. and Steinegger, M., 2022. ColabFold: making protein folding accessible to all. *Nature methods*, 19(6), pp.679-682.
- Molineux, I.J. and Panja, D., 2013. Popping the cork: mechanisms of phage genome ejection. *Nature Reviews Microbiology*, 11(3), pp.194-204.
- Monahan, L.G., Robinson, A. and Harry, E.J., 2009. Lateral FtsZ association and the assembly of the cytokinetic Z ring in bacteria. *Molecular microbiology*, 74(4), pp.1004-1017.
- Natale, P., Pazos, M. and Vicente, M., 2013. The *Escherichia coli* divisome: born to divide. *Environmental microbiology*, 15(12), pp.3169-3182.
- O'Neill, J., 2016. Tackling drug-resistant infections globally: final report and recommendations
- Pan, C.Q., Finkel, S.E., Cramton, S.E., Feng, J.A., Sigman, D.S. and Johnson, R.C., 1996. Variable structures of Fis-DNA complexes determined by flanking DNA-protein contacts. *Journal of molecular biology*, 264(4), pp.675-695.
- Papagiannis, C.V., Sam, M.D., Abbani, M.A., Yoo, D., Cascio, D., Clubb, R.T. and Johnson, R.C., 2007. Fis targets assembly of the Xis nucleoprotein filament to promote excisive recombination by phage lambda. *Journal of molecular biology*, 367(2), pp.328-343.

- Payne, D.J., Miller, L.F., Findlay, D., Anderson, J. and Marks, L., 2015. Time for a change: addressing R&D and commercialization challenges for antibacterials. *Philosophical Transactions of the Royal Society B: Biological Sciences*, 370(1670), p.20140086.
- PDB ID 7n4d
 PDB DOI citation: Sroge, C.D., Davies, D.R., Horanyi, P.S., Lorimer, D.D., Edwards, T.E., Abendroth, J. Translation initiation factor eif-5a family protein from *Naegleria fowleri* ATCC 30863. <https://doi.org/10.2210/pdb7N4D/pdb>
- Rodrigues, C.D. and Harry, E.J., 2012. The Min system and nucleoid occlusion are not required for identifying the division site in *Bacillus subtilis* but ensure its efficient utilization. *PLoS genetics*, 8(3), p.e1002561.
- Rohmer, M., 2008. From molecular fossils of bacterial hopanoids to the formation of isoprene units: discovery and elucidation of the methylerythritol phosphate pathway. *Lipids*, 43(12), pp.1095-1107.
- Romberg, L. and Levin, P.A., 2003. Assembly dynamics of the bacterial cell division protein FtsZ: poised at the edge of stability. *Annual Reviews in Microbiology*, 57(1), pp.125-154.
- Rowlett, V.W. and Margolin, W., 2015. The Min system and other nucleoid-independent regulators of Z ring positioning. *Frontiers in microbiology*, 6, p.145050.
- Rueggeberg, K.G., Toba, F.A., Bird, J.G., Franck, N., Thompson, M.G. and Hay, A.G., 2015. The lysis cassette of DLP12 defective prophage is regulated by RpoE. *Microbiology*, 161(8), pp.1683-1693.
- Schumacher, M.A., Ohashi, T., Corbin, L. and Erickson, H.P., 2020. High-resolution crystal structures of *Escherichia coli* FtsZ bound to GDP and GTP. *Acta Crystallographica Section F: Structural Biology Communications*, 76(2), pp.94-102.
- Semerjian, A.V., Malloy, D.C. and Poteete, A.R., 1989. Genetic structure of the bacteriophage P22 PL operon. *Journal of molecular biology*, 207(1), pp.1-13.
- Sergueev, K., Court, D., Reaves, L. and Austin, S., 2002. *E. coli* cell-cycle regulation by bacteriophage lambda. *Journal of molecular biology*, 324(2), pp.297-307.
- Sergueev, K., Yu, D., Austin, S. and Court, D., 2001. Cell toxicity caused by products of the pL operon of bacteriophage lambda. *Gene*, 272(1-2), pp.227-235.
- Shiomi, D., Mori, H. and Niki, H., 2009. Genetic mechanism regulating bacterial cell shape and metabolism. *Communicative & integrative biology*, 2(3), pp.219-220.
- Silber, N., Matos de Opitz, C.L., Mayer, C. and Sass, P., 2020. Cell division protein FtsZ: from structure and mechanism to antibiotic target. *Future microbiology*, 15(9), pp.801-831.
- Simpkin, A.J. and Rigden, D.J., 2016. GP0. 4 from bacteriophage T7: in silico characterisation of its structure and interaction with *E. coli* FtsZ. *BMC research notes*, 9, pp.1-9.

- Skoko, D., Yoo, D., Bai, H., Schnurr, B., Yan, J., McLeod, S.M., Marko, J.F. and Johnson, R.C., 2006. Mechanism of chromosome compaction and looping by the *Escherichia coli* nucleoid protein Fis. *Journal of molecular biology*, 364(4), pp.777-798.
- Stella, S., Cascio, D. and Johnson, R.C., 2010. The shape of the DNA minor groove directs binding by the DNA-bending protein Fis. *Genes & development*, 24(8), pp.814-826.
- Studier, F.W., 1972. Bacteriophage T7: Genetic and biochemical analysis of this simple phage gives information about basic genetic processes. *Science*, 176(4033), pp.367-376.
- Susskind, M.M. and Botstein, D.A.V.I.D., 1978. Molecular genetics of bacteriophage P22. *Microbiological reviews*, 42(2), pp.385-413.
- Takada, A., Wachi, M. and Nagai, K., 1999. Negative regulatory role of the *Escherichia coli* *hfq* gene in cell division. *Biochemical and Biophysical Research Communications*, 266(2), pp.579-583.
- The PyMOL Molecular Graphics System, Version 1.7.4.5 Schrödinger LLC
- Tommasi, R., Brown, D.G., Walkup, G.K., Manchester, J.I. and Miller, A.A., 2015. ESKAPEing the labyrinth of antibacterial discovery. *Nature reviews Drug discovery*, 14(8), pp.529-542.
- Tran, L., van Baarsel, J.A., Washburn, R.S., Gottesman, M.E. and Miller, J.H., 2011. Single-gene deletion mutants of *Escherichia coli* with altered sensitivity to bicyclomycin, an inhibitor of transcription termination factor Rho. *Journal of bacteriology*, 193(9), pp.2229-2235.
- Vaughan, S., Wickstead, B., Gull, K. and Addinall, S.G., 2004. Molecular evolution of FtsZ protein sequences encoded within the genomes of archaea, bacteria, and eukaryota. *Journal of molecular evolution*, 58(1), pp.19-29.
- Waggoner, B.T., Sultana, K., Symonds, N., Karlok, M.A. and Pato, M.L., 1989. Identification of the bacteriophage Mu *kil* gene. *Virology*, 173(2), pp.378-389.
- Wang, X.D., de Boer, P.A. and Rothfield, L.I., 1991. A factor that positively regulates cell division by activating transcription of the major cluster of essential cell division genes of *Escherichia coli*. *The EMBO journal*, 10(11), pp.3363-3372.
- Westmaas, G.C., van der Maas, W.L. and van de Putte, P., 1976. Defective prophages of bacteriophage Mu. *Molecular and General Genetics MGG*, 145, pp.81-87.
- Wu, L.J., Ishikawa, S., Kawai, Y., Oshima, T., Ogasawara, N. and Errington, J., 2009. Noc protein binds to specific DNA sequences to coordinate cell division with chromosome segregation. *The EMBO journal*, 28(13), pp.1940-1952.
- Yang, S., Pei, H., Zhang, X., Wei, Q., Zhu, J., Zheng, J. and Jia, Z., 2016. Characterization of DicB by partially masking its potent inhibitory activity of cell division. *Open Biology*, 6(7), p.160082.